AN ANALYSIS OF THE RESPONSE OF CYLINDRICAL DUCTS TO INTERNAL, ZERO MEAN FLOW, AIR-CARRIED ACOUSTIC EXCITATION

Author: William T. Ellison

Supervisor: Patrick Leehey
Professor of
Naval Architecture

Submitted: May 17, 1968

AN ANALYSIS OF THE RESPONSE OF CYLINDRICAL DUCTS TO INTERNAL ZERO MEAN FLOW, AIR-CARRIED ACOUSTIC EXCITATION

by

WILLIAM THEODORE ELLISON
LIEUTENANT, UNITED STATES NAVY
B.S., United States Naval Academy
(1963)

Submitted in Partial Fulfillment of the
Requirements for the Degree of
Naval Engineer and the Degree of
Master of Science in Mechanical Engineering
at the
MASSACHUSETTS INSTITUTE OF TECHNOLOGY
May, 1968

ABSTRACT

An Analysis of the Response of Cylindrical Ducts to Internal, Zero Mean Flow, Air-Carried Acoustic Excitation

William Theodore Ellison

Submitted to the Department of Naval Architecture and Marine Engineering on May 18, 1968 in partial fulfillment of the requirements for the Master of Science Degree in Mechanical Engineering and the Professional Degree, Naval Engineer.

Significant structural response of a cylindrical duct to an internal pure tone sound field resulting from an external pure tone source, located approximately on the duct centerline, will arise only when coincidence occurs between the natural modes of propagation of acoustic waves within the duct and the natural modes of structural vibration of the duct itself.

The coupling mechanism giving rise to such coincidence lies within an assumption of small variations of the source location from the duct centerline. This result which arose from a theoretical analysis based on a solution for the velocity potential within a semi-infinite cylinder in the presence of a non-axial incident plane wave and an equivalent modal resonator model of the cylinder undergoing principally radial vibrations in a lobar axially varying

pattern was borne out by the experimental results.

Thesis Supervisor: Patrick Leehey

Title: Professor of Naval Architecture

ACKNOWLEDGMENTS

The author wishes to express his appreciation to Professor P. Leehey for the original proposal of the topic of this thesis and his encouragement in the task of accomplishing the results. The author also wishes to express his thanks to the many persons associated with the Acoustics and Vibration Laboratory, MIT, for their cooperation and assistance in completing the experimental part of this thesis.

The computations presented in this thesis were in part performed at the facilities of the Computation Center, MIT.

TABLE OF CONTENTS

INTRODUCTION

The subject of this thesis lies within the realm of the interaction of structures and sound. The various approachs to sound and structure interaction problems in general fall into one of two categories.

The first which is a relatively new engineering science is one based on the theory of randomness in which classical solutions are often bypassed when meaningful statistical results can be obtained through other approachs. This is a particularly useful analytical tool whenever the structural vibration of interest and/or the sound field of interest exhibit random qualties which allow a statistical analysis of the problem.

The second approach and the one within which the subject of this thesis rightfully belongs, is a direct analysis of a finely structured problem. In the case of this thesis the problem can be stated in general terms as follows; the response of a cylindrical duct to an internal pure tone sound field, where the sound field is the result of an incident puretone plane wave emanating from a source of known location. The problem when stated in such a manner is deceptively simple sounding, for in actuality the complete analytical description of the sound field within a cylindrical duct undergoing asymmetrical vibrations has not been solved in the literature to date. The majority of the papers on the subject of sound within a cylindrical duct contain the assumption that no significant duct

vibration exists. In those papers that take duct vibration into account the assumption is invariably made that the vibration is entirely axially symmetric; a condition which when examined in light of the light of the forces and frequency range involved and other vibration forms possible would be very difficult to bring about. Axially symmetric vibrations of a cylindrical structure involve almost pure stretching energy and are the modes of vibration which they are most likely to resist. It must be noted that this assumption takes on more validity if the structure in question may be termed a membrane (radius to thickness ratios greater than 50).

A form of vibration, however, for which cylindrical structures are uniquely suited is that involving the lobar modes. These are the modes of vibration in which the radial dispacement varies in the circumferential direction in a $\cos(n\theta)$ pattern (n greater than or equal to two). This result first given by Rayleigh (8), is obtainable from a theory based on inextension of the middle surface of the cylinder wall. The next degree of sophistication to Rayleigh's theory of inextensional vibration is one which allows for the presence of axially periodic displacements as well as circumferential ones.

Thus the first purpose of this thesis was to show that if significant vibration of a cylindrical duct could result from an internal sound field, then that vibration must of necessity be an asymmetric one involving the pres-

ence of lobar modes and possibly axial modes as well. The second objective of this thesis was to endeavor to describe the coupling mechanism between this sound field and the cylinder vibration. To accomplish these ends both a theoretical analysis and an experimental analysis were undertaken.

The result of these two analyses show that the form of vibration resulting from an internal sound field was one made up of lobar modes, and that a coupling mechanism based on coincidence of the cylinder structural modes of vibration and the acoustic modes present in the internal sound field does exist and within limits will predict the form of vibration if any that will result from a given sound field.

PROCEDURE

The problem that is posed in this thesis may be subdivided into a number of distinct components, each a dilineated problem within itself and with essence of the final results of the thesis lying within the framework of the interfacial solution matrix of the component parts. The component parts are:

1. A theoretical analysis of sound propagating within a semi-infinite rigid duct, where the sound field is the result of an external pure tone plane wave source offset by a small angle from the duct centerline. This is a classical analytical problem in the area of potential theory. The desired result of this analysis is a description of the sound field within a cylindrical duct at a given frequency. The result is desired only in terms of frequency, source location, and the relative strengths of the different modes.

2. A theoretical analysis of the natural modes of of vibration of a cylindrical duct of finite length. This is a topic with a well-established experimentally validated theory. One of these theories with an approximation based on different end conditions was used in this part of the analysis. The desired result of this component of the problem was the modal form of vibration of a cylinder at a given frequency.

3. An experimental analysis of a steel cylinder of the approximate dimensions; 5 ft. in length, 6 inches in diameter, and ¼ inch in wall thickness, subjected to

a pure tone sound field emanating from a loudspeaker located a distance of approximately 3 ft. from an open end of the cylinder and slightly (2^{o} to 3^{o}) offset from the centerline of the duct axial centerline. The desired result of this component was a frequency versus significant vibration level display for different source locations.

4. Assumptions are the component part which tie together the previous three components. The validity of the final results lies solely within the validity of the assumptions. Basically assumptions played the following roles.

In the 'theoretical sound analysis/experimental analysis' interface they took the form of adapting the experimental model to fit the requirements of the assumptions of the theoretical analysis.

In the 'theoretical analysis of cylinder vibration/ experimental analysis' interface they played the opposite role of adapting the theory to fit the experimental model.

In the interface between the two portions of the theoretical analysis the assumptions took the form of superposition rather than adaption. Thus the superposition of the two separately conceived theories defined a coupling mechanism based on coincidence of the acoustic and structural modes at a given frequency.

5. Analysis of results is the component part which

is the interfacing mechanism between the combined theoretical results and the ensuing experimental results. This interface is examined only in the light of the assumed variables.

6. Conclusions and Recommendations make up the component part which decides the exact nature of the interfacial solutions, their relative strengths and weaknesses and finally of deciding what results are basic to the problem as a whole, i.e. has the basic purpose of the thesis been accomplished. This is done in light of both assumptions and the assumed variables.

THEORETICAL ANALYSIS

I. Theory of Sound Propagation in Cylindrical Ducts

A considerable amount of literature has been devoted to the general problem of the propagation of sound in ducts. The general form for the solution of the wave equation utilizing potential theory as it is presented in the following analysis can be found in Morse (1).

The general solution for the velocity potential within a semi-infinite cylindrical duct of zero wall thickness, when that potential is the result of an incident pure tone plane wave emanating from a non-axial source, is given by Noble (2). Noble structures the problem for solution by a standard Weiner-Hopf technique. In the following analysis it will be shown that a more direct solution is possible if the external field is neglected and the incident wave is assumed to act as a massless asymmetric piston at the source end of the cylindrical duct.

A. Solution of the Wave Equation

Using the space coordinate system shown in Figure I define a region within an infinite acoustic medium,

$$0 \leq r \leq a$$

$$0 \leq z \leq \infty .$$

Further assume that within that region that the velocity potential,

$$\Psi_T(\vec{r},t) = \Psi_T(r,\theta,z,t)$$

Figure I

Space Coordinate System

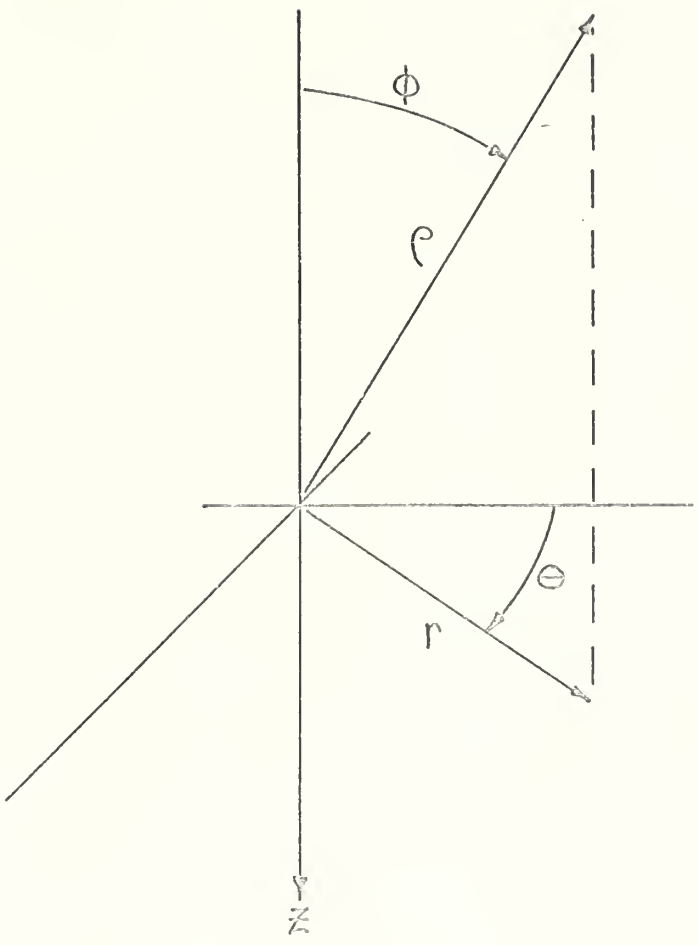

satisfies the linear wave equation of acoustics,

$$\nabla^2 \psi_T - \frac{1}{c_0^2} \frac{\partial^2 \psi_T}{\partial t^2} = 0 , \qquad (1)$$

where ∇^2 is the Laplacian operator in cylindrical coordinates, t is the time coordinate, and c_0 is the velocity of sound in the acoustic medium.

Now assume that $\psi_T(\vec{r},t)$ may be represented by the infinite Fourier transform,

$$\psi_T(\vec{r},t) = \frac{1}{2\pi} \int_{-\infty}^{\infty} \Phi_T(\vec{r},\omega) \exp[-i\omega t]\, d\omega , \qquad (2)$$

where $\Phi_T(\vec{r},\omega)$ is the frequency transform of the velocity potential. Similarly let $\Phi_T(\vec{r},\omega)$ be given by the inverse transform,

$$\Phi_T(\vec{r},\omega) = \int_{-\infty}^{\infty} \psi_T(\vec{r},t) \exp[i\omega t]\, dt . \qquad (3)$$

Then it can be shown that application of Eq.(2) to Eq.(1) will yield the result,

$$\nabla^2 \Phi_T + K^2 \Phi_T = 0 , \qquad (4)$$

where the wavenumber, K, is defined by,

$$K = \frac{\omega}{c_o} \,. \tag{5}$$

It can be shown that the general solution of Eq.(4) for waves propagating in the positive z direction is given by the sum of all modes of oscillation,

$$\Phi_r(\vec{r},\omega) = \sum_{p=0}^{\infty}\sum_{q=1}^{\infty} J_p(\gamma_{pq} r)\cdot \tag{6}$$

$$\cdot\left[A_{pq}(\omega)\cos p\theta + B_{pq}(\omega)\sin p\theta\right]\exp\left[i K_{pq} z\right] ,$$

where p, q are positive integers, $J_p(\ )$ is the Bessel function of the first kind, of integer order p, and K_{pq} is defined by the relation,

$$K_{pq} = \left[K^2 - \gamma_{pq}^2\right]^{1/2} . \tag{7}$$

Now if the surface,

$$r = a \quad ; \quad 0 \le z \le \infty ,$$

is assumed to be rigid then it follows that Φ_r must satisfy the boundary condition,

$$\frac{\partial \Phi_r}{\partial r} = 0 \,, \quad r = a \,, \; 0 \le z \le \infty \,. \tag{8}$$

Now the application of Eq.(8) to Eq.(6) will yield,

$$\frac{\partial J_p(\gamma_{pq} a)}{\partial (\gamma_{pq} a)} = 0 \tag{9}$$

where $\gamma_{pq} a$ is the q^{th} root of Eq.(9). Thus γ_{pq} has been determined for all p,q. Now if a cutoff frequency, f_{pq}, is defined to be,

$$f_{pq} = \frac{c_0}{2a}\left(\frac{\gamma_{pq} a}{2\pi}\right) \tag{10}$$

then Eq.(7) for the mode wavenumber, K_{pq}, may be represented by,

$$K_{pq} = K\left[1 - \left(\frac{f_{pq}}{f}\right)^2\right]^{1/2} \tag{11}$$

where,

$$f = \frac{\omega}{2\pi} \tag{12}$$

It can readily be seen then that for frequencies below the cutoff frequency for a given mode that the mode wavenumber is imaginary and therefore the mode is highly damped and will not propagate. At frequencies greater than the cutoff frequency Eq.(11) yields a real result and the mode will propagate in the positive Z direction with the wavenumber specified by Eq.(11).

B. Determination of A_{pq} and B_{pq} .

Assume that within the region specified by,

$$-\infty \leq z \leq 0$$

there exists a pure tone plane wave source such that the axis of incidence of the plane wave on the the point,

$$r = 0 \; ; \; z = 0$$

is specified by two quantities θ_0 and ϕ_0 ; see Figure II. Further let Ψ_i , represent the frequency transform of the unit velocity potential of this incident wave in the region, $-\infty \leq z \leq 0$. Now if it is assumed that Ψ_T must vanish in the region,

$$a \leq r \leq \infty$$

$$0 \leq z \leq \infty$$

then it can be shown that on the surface specified by,

$$0 \leq r \leq a$$

$$z = 0$$

Ψ_i must act as an asymmetric massless piston on the region,

$$0 \leq r \leq a$$

$$0 \leq z \leq \infty$$

Determination of A_{pq} and B_{pq} may then be accomplished in the following manner. If Eq.(6) is multiplied successively by $J_p(\gamma_{pq} r) \cos p\theta$ and $J_p(\gamma_{pq} r) \sin p\theta$

Figure II
Source Position

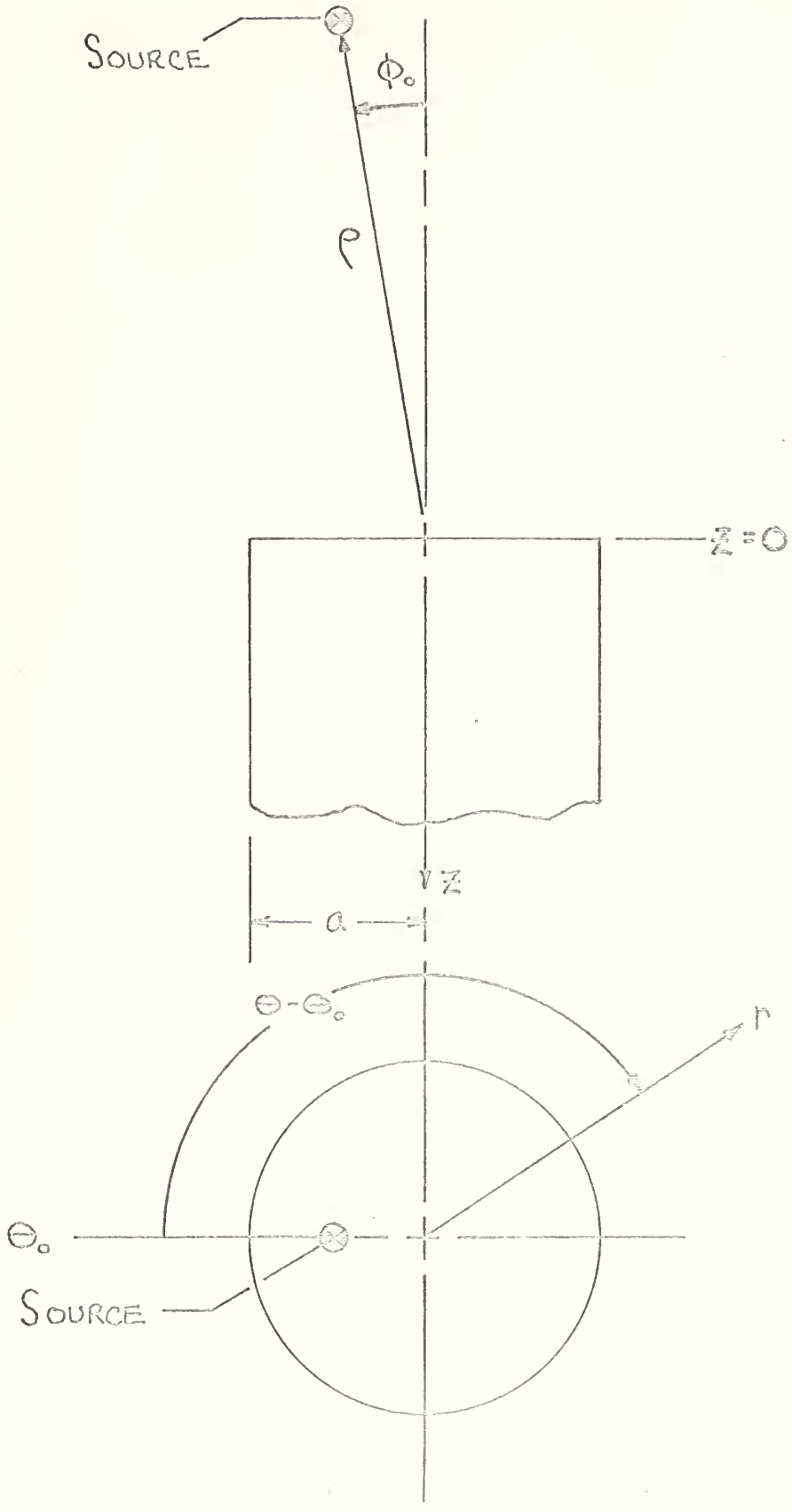

and the result integrated over the plane, $z = 0$, it is seen that a non-zero result is obtained only for the surface area specified by,

$$0 \leq r \leq a$$
$$z = 0$$

Thus the following relation is obtained,

$$\left.\begin{matrix} A_{pq} \\ B_{pq} \end{matrix}\right\} = \int_0^a r\,dr\, \frac{J_p(\gamma_{pq} r)}{\Gamma_{pq}} \cdot \int_0^{2\pi} d\theta\, \Psi_r(r,\theta,0,\omega) \left\{\begin{matrix} \cos p\theta \\ \sin p\theta \end{matrix}\right.$$

where,

$$\Gamma_{pq} = \pi a^2 \epsilon_p J_p^2(\gamma_{pq} a)\left[1 - \left(\frac{p}{\gamma_{pq} a}\right)^2\right]$$

$$\epsilon_p = \begin{cases} 1 & p = 0 \\ 1/2 & p \geq 1 \end{cases}$$

But assuming that the effect of the incident is to act as a massless asymmetric piston on the this region then it must follow that,

$$\Psi_r(r,\theta,0,\omega) = \Psi_i(r,\theta,0,\omega); \quad 0 \leq r \leq a$$

and as a result,

$$\left.\begin{matrix} A_{pq} \\ B_{pq} \end{matrix}\right\} = \frac{1}{\Gamma_{pq}} \int_0^a r\,dr\, J_p(\gamma_{pq} r) \cdot \int_0^{2\pi} d\theta\, \Psi_i(r,\theta,0,\omega) \left\{\begin{matrix} \cos p\theta \\ \sin p\theta \end{matrix}\right. \qquad (13)$$

Now using the notation of Figure II and assuming that $\theta_o = 0$, with no loss in generality, then the unit incident velocity potential is given by,

$$\psi_i(\vec{R},t) = \exp\Big[i k \rho \Big[\cos\phi\cos\phi_o + \sin\phi\sin\phi_o\cos\theta \Big] \Big] \cdot \exp\big[-i\omega t\big] \tag{14}$$

and using the well known result,

$$e^{-iv\cos\Theta} = \sum_{m=-\infty}^{\infty} (-i)^m e^{-im\Theta} J_m(v)$$

where $J_m(v)$ is the Bessel function of the first kind of integer order m , then Eq.(14) may be rewritten as

$$\psi_i(\vec{R},t) = e^{i(kz\cos\phi_o - \omega t)} \cdot \sum_{m=-\infty}^{\infty} (-i)^m e^{-im\theta} J_m(kr\sin\phi_o) \tag{15}$$

Now taking the Fourier transform of Eq.(15),

$$\Psi_i(\vec{R},\omega) = \int_{-\infty}^{\infty} \psi_i(\vec{R},t)\, e^{i\omega t}\, dt$$

it can be shown that,

$$\Psi_i(\vec{R},\omega) = 2\pi\delta(\omega-\omega')\, e^{ikz\cos\phi_o} \cdot \sum_{m=-\infty}^{\infty} (-i)^m e^{-im\theta} J_m(kr\sin\phi_o) \tag{16}$$

where $\delta(\omega-\omega')$ is the unit impulse function. Now assuming that ϕ_o is a small angle such that,

$$\cos\phi_o \sim 1$$
$$\sin\phi_o \sim \phi_o$$

then it can be shown that by applying Eq.(16) to Eq.(13) the following results,

$$\left.\begin{matrix} A_{pq} \\ B_{pq} \end{matrix}\right\} = \frac{2\pi\delta(\omega-\omega')}{\Gamma_{pq}} \int_0^a r\,dr\, J_p(\gamma_{pq}r) \cdot$$
$$\cdot \int_0^{2\pi} d\theta \sum_{m=-\infty}^{\infty} (-i)^m e^{-im\theta} J_m(kr\phi_o) \left\{\begin{matrix} \cos p\theta \\ \sin p\theta \end{matrix}\right.$$

Examining the integration over $\int d\theta$ first, it can be seen that the result is non-zero only for $p = \pm m$ and knowing that $J_{-m} = (-1)^m J_m$ then it can be shown that,

$$\left.\begin{matrix} A_{pq} \\ B_{pq} \end{matrix}\right\} = \frac{2\pi\delta(\omega-\omega')}{\Gamma_{pq}} \int_0^a r\,dr\, J_p(\gamma_{pq}r)\, J_p(k\phi_o r) \cdot$$
$$\cdot 2 \int_0^{2\pi} (-1)^p (i)^p \cos p\theta \left\{\begin{matrix} \cos p\theta \\ \sin p\theta \end{matrix}\right\} d\theta$$

Now upon performing the integration $2\cdot\int_0^{2\pi} d\theta(\ )$ it must follow that B_{pq} is zero for all p,q, and that

$$A_{pq} = \frac{4\pi^2 \delta(\omega-\omega')(-1)^p(i)^p}{\Gamma_{pq}} \int_0^a J_p(\gamma_{pq}r) J_p(k\phi_0 r) r\, dr$$

Now define a quantity β, such that,

$$\beta = ka\phi_0 \tag{21}$$

Then it can be shown that the remaining integration over $\int_0^a dr(\ )$ will yield a convergent infinite series in powers of β. The result of this integration for the four principle modes of interest is given below, (the series has been truncated to yield accuracy to the fourth significant figure for $\beta < 1$)

$$A_{01} = \pi\delta(\omega-\omega')\frac{J_1(\beta)}{\beta} \tag{22}$$

$$A_{21} = -4\pi\delta(\omega-\omega')\left[.0949\beta^2 - .0046\beta^4\right] \tag{23}$$

$$A_{31} = i\,4\pi\delta(\omega-\omega')\left[.0791\beta^3 - .0031\beta^5\right] \tag{24}$$

$$A_{41} = 4\pi\delta(\omega-\omega')\left[.6334\beta^4 - .0334\beta^6\right] \tag{25}$$

Now within the region,

$$0 \leq r \leq a$$
$$0 \leq z \leq \infty$$

the sound pressure $P(\vec{r},t)$ is related to the velocity potential in the following way,

$$P(\vec{r},t) \sim \frac{\partial}{\partial t} \Psi_T(\vec{r},t) \tag{26}$$

and similarly it follows that the frequency transform of the pressure within this region is given by,

$$P(\vec{r},\omega) \sim i\omega \Phi_T(\vec{r},\omega)$$

and it therefore follows that,

$$P(\vec{r},t) \sim \frac{1}{2\pi} \int_{-\infty}^{\infty} i\omega \Phi_T(\vec{r},\omega) e^{-i\omega t} d\omega \tag{27}$$

Now upon application of Eq.(6) to Eq.(27) it must result that,

$$P(\vec{r},t) \sim \sum_{p=0}^{\infty} \sum_{q=1}^{\infty} J_p(\gamma_{pq} r) \int_{-\infty}^{\infty} A_{pq} \cos p\theta \, e^{i(k_{pq} z - \omega t)} \omega \, d\omega \tag{28}$$

Where the A_{pq} of interest are given by Eq.'s (22) through (25).

A result to be needed later in tnis analysis is $P(r,\theta,z,t)$ evaluated at $r=a$. This quantity then must be of the form,

$$P(a,\theta,z,t) \sim \sum_{p=0}^{\infty}\sum_{q=1}^{\infty} G_{pq}(\omega,\beta)\cos p\theta \cdot \tag{29}$$

$$J_p(\gamma_{pq}a)\cdot \exp[i\kappa_{pq}z - i\omega t]$$

where,

$$G_{21} = \omega\left[.0949\beta^2 - .0046\beta^2\right] \tag{30}$$

$$G_{31} = i\omega\left[.0791\beta^3 - .0031\beta^5\right] \tag{31}$$

$$G_{41} = \omega\left[.6334\beta^4 - .0334\beta^6\right] \tag{32}$$

II. Theory of Vibration of Hollow Cylinders

A considerable amount of literature exists on the theory of vibration of hollow cylinders, particularly in the area of calculation techniques for determining the natural modes of vibration. Greenspon (3) has compiled a synopis of the vast majority of these theories and has compared them on the basis of their variance from the exact theory and in their ability to predict experimental results accurately. It was found that for the duct dimensions and range of frequencies considered in the experimental portion of this paper that a large number of theories gave excellent results. The theory that was chosen was that of Arnold and Warburton (4), primarily on the basis that it lent itself to a computerized solution.

A. The Arnold and Warburton Theory

The Arnold and Warburton theory is confined to those modes of cylinder vibration in which bending and stretching of the shell predominate. Over the range of frequencies and cylinder physical parameters examined in this paper, the bending energy was predominately the energy involved in the vibrations and the radial direction of vibration the predominate direction of displacement. For simplification the rest of this section will deal only with the radial modes of vibration due to their predominance in the lower frequencies. Basically in the lower range of natural cylinder frequencies of vibration Arnold and Warburton have solved the two-dimensional problem of

Rayleigh (8), utilizing Timoshenko's (7) strain relations and neglecting the trapezoidal shape of the incremental surfaces perpendicular to the cylinder axis. This analysis allows for the presence of axial nodes as well as circumferential nodes, whereas Rayleigh's theory does not. It is of note however that their theory gives the same resonant frequencies as Rayleigh's for the case of no axial nodes.

A difficulty presented itself in that Arnold and Warburton solved the above problem where the ends of the cylinder in question were freely supported. The end conditions of the cylinder which was the basis for the experimental portion of this thesis were not freely supported but rather approximated the condition of a free end and an indeterminate end condition. Using the coordinate system of Figure II Arnold and Warburton assumed that the radial displacement was of the following form,

$$W(\theta,z) = W_0 \cos n\theta \cos \frac{m\pi z}{2L} \qquad (33)$$

where m is the number of quarter wavelengths in the axial vibration pattern and n is the number of full wavelenghths in the circumferential wave pattern. Thus it can be seen that this shape function satisfies the condition of circularity at the cylinder ends necessary for freely supported end conditions. As stated above,

however, the cylinder which was used in the experimental portion of this problem was not supported in this manner, rather the end nearest the sound source was a free end and the other approximated another free end, that end being imbedded in sand of a large grain size variety to a depth of several inches. An approximation therefore had to be made to adapt the Arnold and Warburton frequency equation to the cylinder of this problem. The approximation was arrived at in the following manner.

If it is assumed that the general form of the radial displacement in the axial pattern is given by,

$$\frac{U(z)}{U_0} = C_1\left(\cos\frac{m\pi z}{2L} + \cosh\frac{m\pi z}{2L}\right) + C_2\left(\cos\frac{m\pi z}{2L} + \cosh\frac{m\pi z}{2L}\right) + C_3\left(\sin\frac{m\pi z}{2L} + \sinh\frac{m\pi z}{2L}\right) + C_4\left(\sin\frac{m\pi z}{2L} - \sinh\frac{m\pi z}{2L}\right) \quad (34)$$

then the requirement of of a free end at $z=0$ requires,

$$\frac{\partial^2 U}{\partial z^2} = 0 \quad ; \quad z=0 \quad (35)$$

$$\frac{\partial^3 U}{\partial z^3} = 0 \quad ; \quad z=0 \quad (36)$$

In order for Eq.(34) to satisfy Eq.(35) and Eq.(36) it must follow that C_2 and C_4 are identically zero, or that,

$$\frac{U(z)}{U_0} = C_1\left(\cos\frac{m\pi z}{2L} + \cosh\frac{m\pi z}{2L}\right) + C_3\left(\sin\frac{m\pi z}{2L} + \sinh\frac{m\pi z}{2L}\right) \quad (37)$$

Now a shape function which yields the same resultant frequency equation as the Arnold and Warburton theory and which also approximates Eq.(37) for m large is given by,

$$\frac{W(z,\theta)}{W_0} = \cos n\theta \cdot \frac{1}{\sqrt{2}}\left(\cos\frac{m\pi z}{2L} - \sin\frac{m\pi z}{2L}\right) \qquad (38)$$

It is seen that for large m that this is closely approximated by Eq.(37) with,

$$C_1 = -C_3 = \frac{1}{\sqrt{2}}$$

$$e^{-\frac{m\pi z}{2L}} \sim 0$$

It is easier to visualize this approximation when it is realized that for a large number of nodes a " free-free " vibration is equivalent to one described by Eq.(38) with m an odd integer, but with the supports each displaced toward the center of the cylinder an eighth of a wave length, and the number of waves between these two imaginary supports being an integer number of half wave lenghths. Thus if an axial wave length factor, λ , is defined such that,

$$\lambda = \frac{m\pi\bar{a}}{2L} \qquad (39)$$

then for large m , λ , will have the same value

at a given frequency for either set of end conditions, for though the effective length has been reduced by a quarter of a wave length,

$$L' = L\left(1 - \frac{1}{m}\right)$$

so also has the effective number of wave lengths been reduced by the same factor,

$$m' = m\left(1 - \frac{1}{m}\right)$$

A computerized solution of the Arnold and Warburton frequency equation is given in Appendix B , where λ in the output is represented by the letter K.

B. The Equivalent Resonator for a Structural Mode

Smith and Lyon (5) outline a method by which a structural system vibrating in a single resonant mode may be modeled by an equivalent resonator with an equivalent mass, damping constant, and spring constant.

Consider a cylinder of mean radius, $\bar{a}$, length, L , and density, ρ_o . Then using the coordinate system of Figure II with $\Theta_o = 0$, and the mode shape defined in Eq.(38) then the instantaneous displacement in the radial direction may be given by,

$$W(\bar{a},\Theta,z,t) = W_{mn}(t)\,\frac{C_{mn}}{\sqrt{2}}\cos n\Theta \cdot \left[\cos\frac{m\pi z}{2L} - \sin\frac{m\pi z}{2L}\right] \tag{40}$$

Similarily let the instantaneous velocity in the radial direction be represented by,

$$V(\bar{a},\Theta,z,t) = V_{mn}(t)\,\psi_{mn}(\bar{a},\Theta,z) \tag{41}$$

where,

$$\psi_{mn}(\bar{a},\Theta,z) = \frac{C_{mn}}{\sqrt{2}}\cos n\Theta \cdot \left(\cos\frac{m\pi z}{2L} - \sin\frac{m\pi z}{2L}\right) \tag{42}$$

is a shape function. If it is then required that the shape function be normalized in such a way that the integral of

the shape function over the volume of the cylinder be equal to the mass of the cylinder, e.g.,

$$\int_{\forall} \rho_0 \left| \xi_{mn} \right|^2 d\forall = M_0 \tag{43}$$

then it follows that,

$$C_{mn} = \sqrt{2}$$

It can be seen that the kinetic energy, T , associated with a given mode of vibration can be represented by,

$$T = \frac{1}{2} M_0 V_{mn}^2 (t) \tag{44}$$

In the same sense a modal spring constant may be defined to be,

$$K_{mn} = \omega_{mn}^2 M_0 \tag{45}$$

and a modal resistance, $R_{mn,INT}$, such that,

$$\Pi = R_{mn,INT} V_{mn}^2 (t) \tag{46}$$

where in a given vibration Π is the total power dissipated internal to the structure.

III. The Coupling Parameter

In the preceding section an equivalent modal resonator was defined by a set of parameters that describe the vibration of the structure of interest at any given frequency, ω_{mn} .

Next define an equivalent modal force, $f_{mn}(t)$, such that the instantaneous power supplied to the resonator is identical with the modal component of total power delivered to the structure (5). In the present analysis where the power delivered to the structure is that due to the internal sound field in the cylinder then the identity of instantaneous powers is given by,

$$f_{mn}(t)\, V_{mn}(t) = \int_S P(\vec{r},t)\, V_{mn}(t)\, \psi_{mn}(\vec{r})\, ds \qquad (47)$$

where the integral implies the the integral over the interior surface of the cylindrical duct. Assuming that the pressure $P(\vec{r},t)$ can be expressed as the superposition of two parts,

$$P(\vec{r},t) = P_{BL}(\vec{r},t) + P_{RAD}(\vec{r},t) \qquad (48)$$

then the first, $P_{BL}(\vec{r},t)$, is that pressure which would exist in the cylinder in the absence of structural motion, i.e., a pressure of the type given by Eq.(29). The second part, , is that due solely to non-vanishing structural motion. This decoupling of the two parts of

the sound field is valid if it is assumed that the coupling of other non-resonant modes will not occur. This is particularly true for the vibration of structures in air, the case being examined here, as the density of the structure undergoing vibration is usually many times greater than the density of air. If it is assumed that Eq.(48) is a valid assumption then it follows that the modal force may be decoupled in a similar fashion to yield,

$$f_{mn,BL}(t) = \int_S P_{BL}(\vec{r},t)\, \xi_{mn}(\vec{r})\, dS \qquad (49)$$

Now knowing that the sound field of interest is pure tone it can be stated that,

$$f_{mn,BL}(t) = F_{mn,BL} \cdot e^{-i\omega_{mn}t} \qquad (50)$$

where $F_{mn,BL}$ is the total blocked force, and it must also follow that,

$$F_{mn,BL}\, e^{-i\omega_{mn}t} \sim P_o\, e^{-i\omega_{mn}t} \qquad (51)$$

where P_o is the amplitude of the internal sound field. By application of Eq.(51) to Eq.(49) a coupling parameter

χ_{mn}, may be defined to express the ratio between the blocked force and the incident sound pressure on the interior of the cylinder, such that,

$$\chi_{mn} = \frac{F_{mn,BL}}{P_0} = \int_S \frac{P_{BL}(\vec{R})}{P_0} \psi_{mn}(\vec{z})\, ds \qquad (52)$$

Now $\psi_{mn}(\vec{R})$ is given by Eq.(42) and $\frac{P_{BL}(\vec{R})}{P_0}$ is given by the non time dependent part of Eq.(29). Thus Eq.(52) may be represented by,

$$\chi_{mn} = \int_0^L a\, dz \sum_{p=0}^{\infty}\sum_{q=1}^{\infty} \left\{ \left(\cos\frac{m\pi z}{2L} - \sin\frac{m\pi z}{2L}\right) e^{\cdot iK_{pq}z} \cdot \left(J_p(\gamma_{pq}a)\Theta_{pq}(\beta)\right) \int_0^{2\pi} \cos p(\theta-\theta_0)\cos n(\theta-\theta_0)\, d\theta \right\} \qquad (53)$$

where for generality θ_0, in the sense of Figure II, has been reinserted. It is then a simple matter to show that the coupling parameter, χ_{mn}, is non-zero only for $n = p$, in which case Eq.(53) takes the form,

$$\chi_{mn} = \pi a \int_0^L dz \sum_{q=1}^{\infty} \left\{ \left(\cos\frac{m\pi z}{2L} - \sin\frac{m\pi z}{2L}\right) e^{\cdot iK_{nq}z} \cdot J_n(\gamma_{nq}a)\Theta_{nq}(Ka\phi_0) \right\} \qquad (54)$$

Further it can be shown that significant values of corresponding to efficient coupling of the sound field and the cylinder vibration are achieved only when,

$$K_{nq} = \frac{\lambda}{a} = \frac{m\pi}{2L} \qquad (55)$$

IV. Theoretical Conclusions

Eq.(54), the coupling parameter, when combined with a solution to the natural modes of vibration of a cylinder is the basic result of the theoretical portion of this thesis. This result is shown graphically in Figure III. The ordinate variable, $\Delta^{1/2}$, is a dimensionless frequency parameter defined by,

$$\Delta^{1/2} = f\left(\frac{4\pi^2 \bar{a}^2 \rho_0 (1-\sigma^2)}{Eg}\right)^{1/2} \qquad (56)$$

(f is the frequency in KC)

where σ is Poisson's ratio and E is Young's modulus. The abcissa variable is the axial wave length factor, λ , defined by Eq.(39). The solid lines represent solutions to the Arnold and Warburton frequency equation for the cylinder that was the subject of the experimental analysis of this thesis in that they represent the loci of of modes of vibration having equal number of circumferential nodes. The dotted lines represent the requirement of Eq.(55) which may be combined with Eq.(11) to yield the relation,

$$K_{pq} = \frac{2\pi f}{c}\left[1 - \left(\frac{f_{pq}}{f}\right)^2\right]^{1/2} = \frac{\lambda}{\bar{a}} \qquad (57)$$

and are plotted for the (p,q) modes: (2,1), (3,1),& (4,1). Thus it must follow that significant coupling will

occur only when the (p,1) dotted lines intersect the corresponding $p=n$ solid lines. This occurence is indicated where it occurs on the Figure by a $\bigcirc$.

Figure III

Prediction of points of high coupling efficiency.

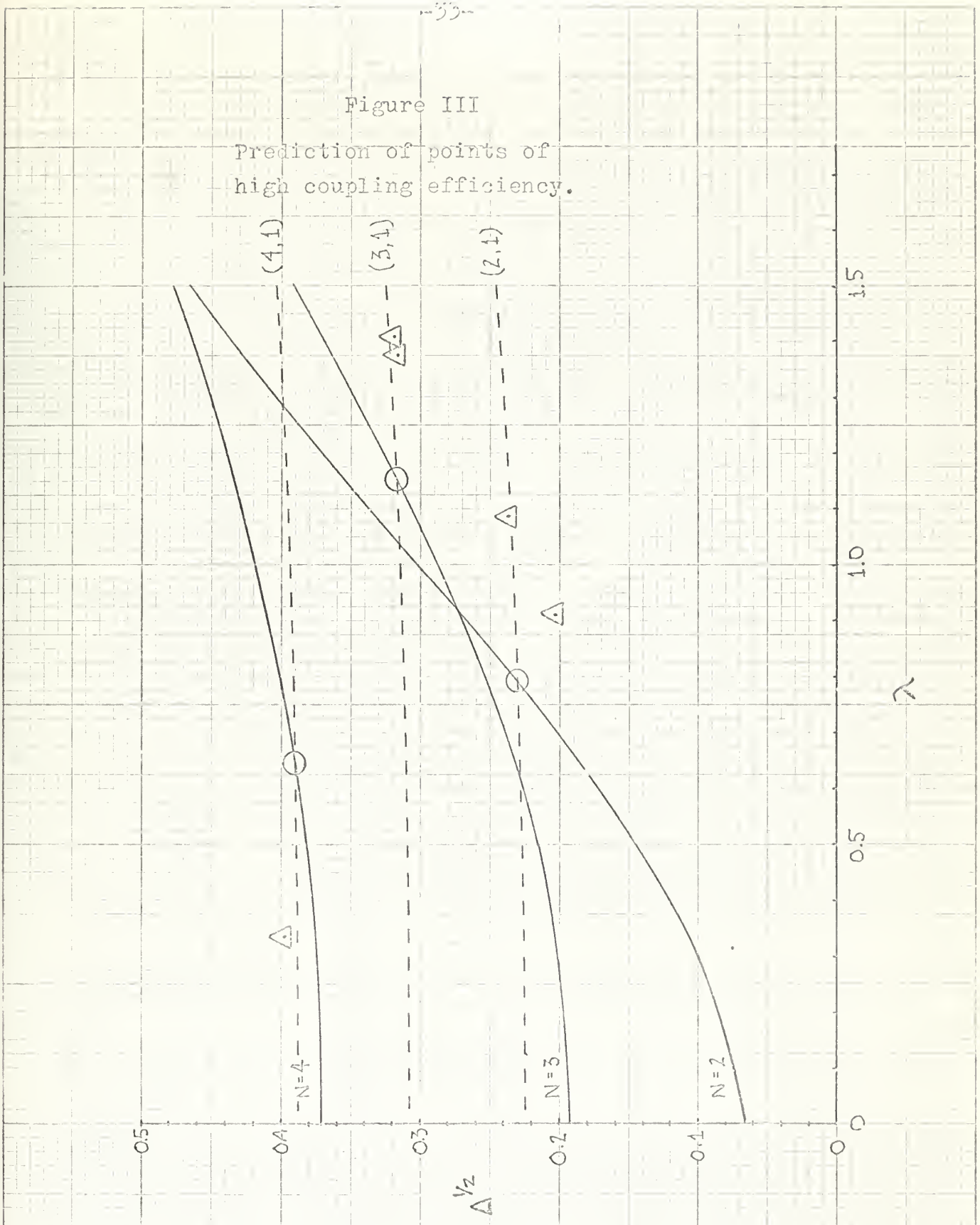

EXPERIMENTAL ANALYSIS

The purpose of the experimental analysis was to show experimentally that an internal sound field could excite structural resonances in a cylindrical duct and that those modes excited would be lobar type modes.

The form of the experimental model which was created to accomplish this purpose depended to a great extent on the assumptions made in the theoretical analyses. The first section of the experimental analysis therefore deals solely with these assumptions and their effect upon the experimental model.

I. Discussion of Theoretical Assumptions

The following discussion centers only on the four major assumptions of the theory which had to be met in order for any valid comparison to be made between the theoretical and experimental results.

A. "Sound field restricted to interior of the cylindrical duct..."

Figure IV shows a scale plan of the experimental model. The speaker was surrounded completely by two layers of three inch fiberglass blanketing on the vertical sides and three layers on the top and bottom. The whole was held together by thin wooden studding along the outside edges to insure that no significant solid boundaries were presented to the sound field with the exception of the interior walls of the duct. This cage-like structure was then freely suspended from a steel ring anchored in

Figure IV

Experimental Model

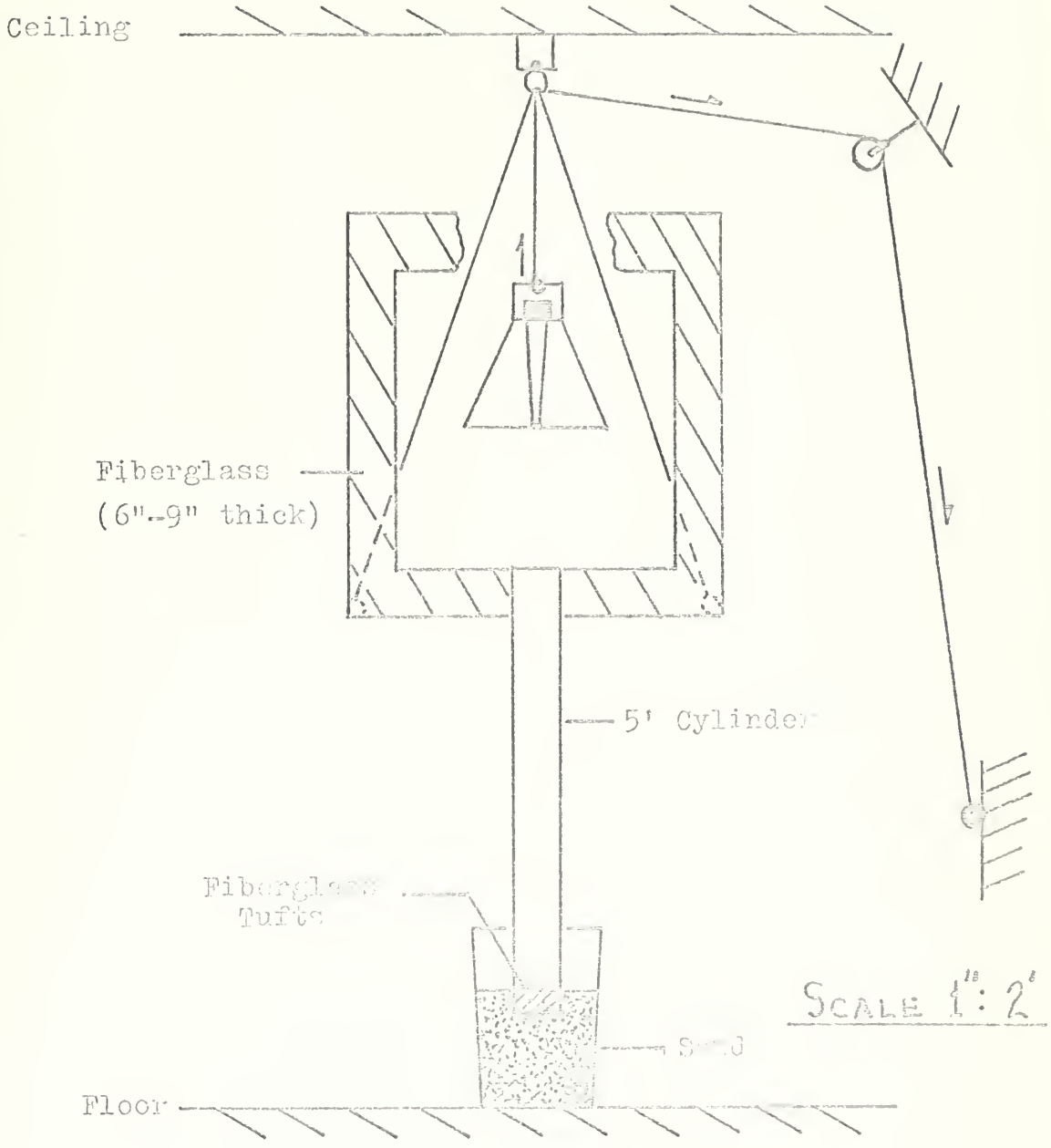

the ceiling. The cylinder mouth was exposed to the sound field by cutting a hole of the exact size of the cylinder outside diameter in the bottom of the speaker enclosure and then arranging the two so that the end of the cylinder was flush with the inner layer of insulation and snugly fitted by it as shown in Figure IV. It was found however that the sound dampening characteristics of the insulation were not of an efficient nature for frequencies below 1900 Hz. Below this frequency there existed a significant external sound field. A cylinder vibration mode corresponding to the lowest natural lobar mode of the cylinder was excited at a frequency of 720 Hz; however it was discovered that significant changes in the acceleration levels being recorded could be achieved simply by the movement of persons or objects in close proximity to the cylinder. This same phenomena was not present at frequencies above 1900 Hz.

B. " Duct acoustically semi-infinite in length..."

This assumption led to the placement of tufts of insulation material to a depth of six inches in the bottom of the cylinder. Based on the experience with the external sound field described above it was then assumed that at frequencies above 1900 Hz that no significant reflection of incident waves occurred at the bottom termination of the cylinder, thus allowing only waves propagating in the positive Z direction.

C. "Pure tone plane wave source..."

The input to the driver element of the speaker was an amplification of the output of a pure tone oscillator. The driver element to duct mouth distance used in the experimental data to be presented was approximately three feet corresponding to a value of, (see Figure V)

$$K\rho \sim 29$$

thus satisfying the requirement of $K\rho >> 1$ necessary for the assumption of a plane wave source.

D. "Source offset from centerline of duct by a small angle..., and $\beta < 1$ ...."

Due to the physical characteristics of the model the offsetting of the source location from the duct axial centerline was accomplished in a reverse manner by inclining the cylinder to a given angle and then readjusting the whole such that the center of the top of the duct was directly beneath the the source. Measurements of the inclined angle were accomplished with a plumb bob device. The angular offsets used were 2° and 3° thus resulting in a value for β of approximately 0.3 ,(See Figure VI), thus satisfying the requirement of $\beta < 1$.

E. "Cylinder end conditions of 'Free - Indeterminate' in experimental model..."

The upper end of the duct was truly a free end in that it was in no way supported by the insulating enclosure. The bottom end was imbedded in sand to a depth of

Figure V

Variation of Kρ
with Speaker Location
and Frequency

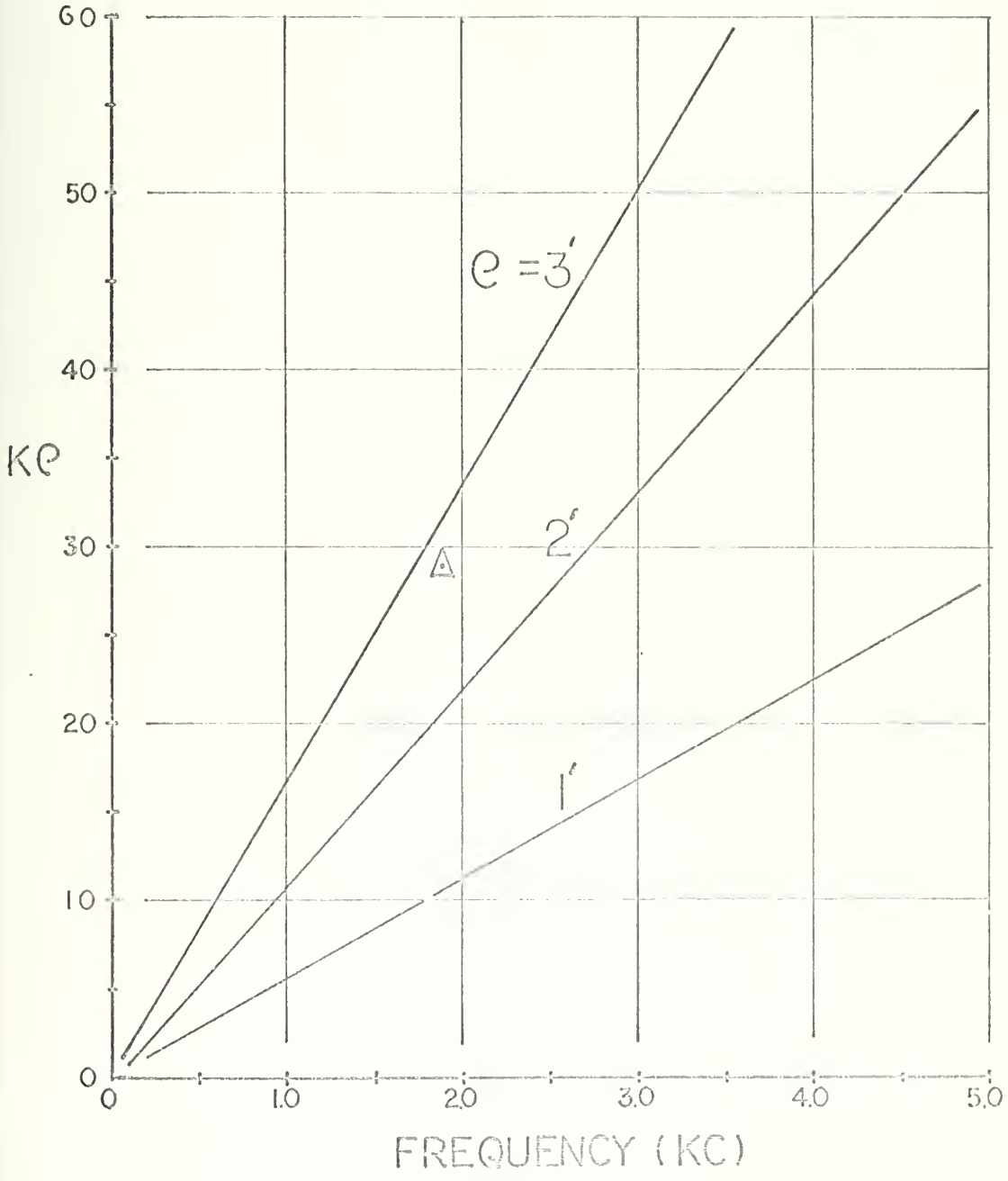

Figure VI

Variation of β with Speaker Location and Frequency

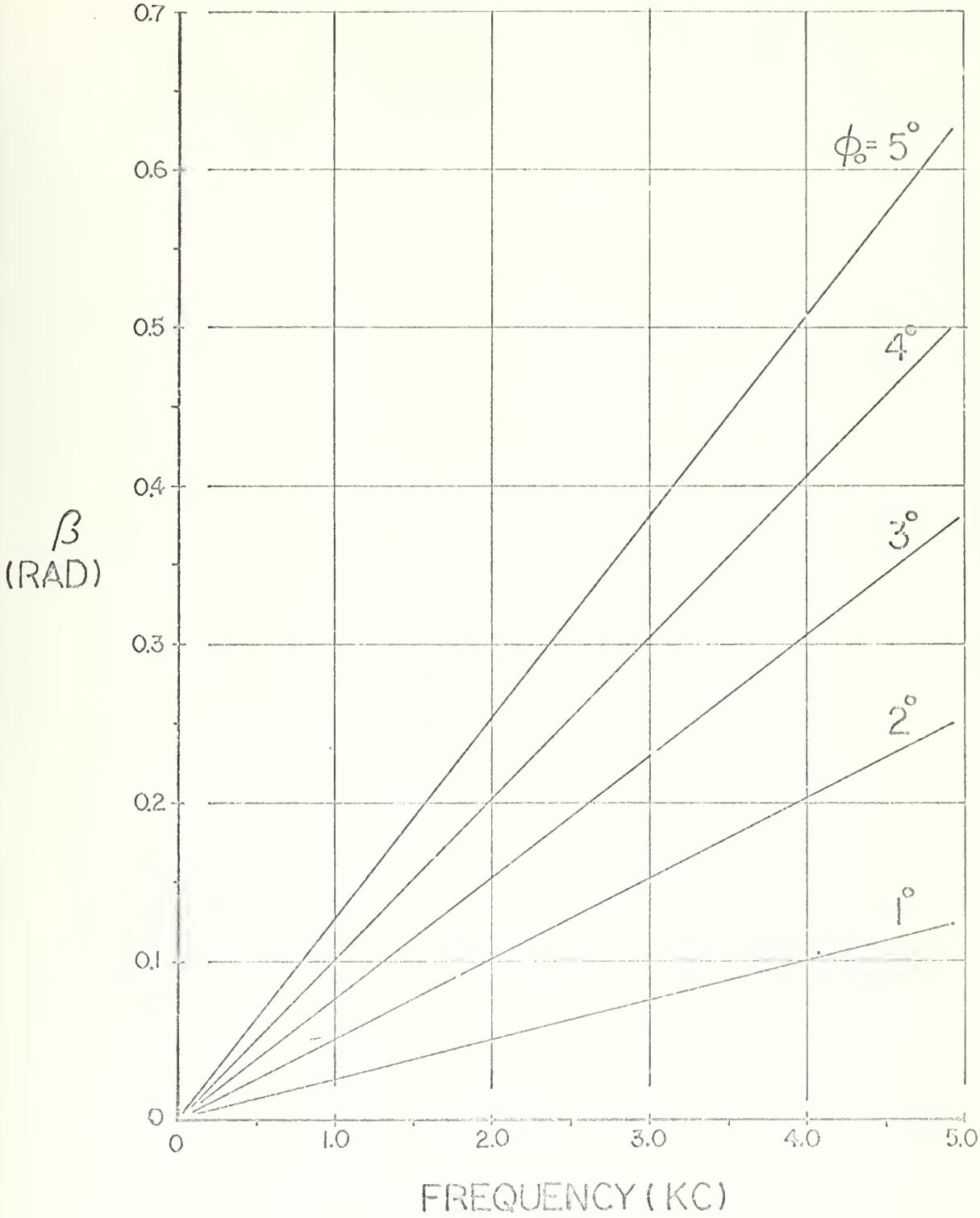

several inches. The sand could probably be better termed small grained gravel in that it supplied sufficient holding force to support small offset angles when the cylinder was inclined but could not have been of much support when trying to oppose high frequency oscillations on the order of microinches. Thus the end condition for this end must be termed indeterminate.

A table of the properties of the cylinder used in the experiment is given in Table I.

Table I

Cylinder Properties

Property	Symbol	Quantity
Length	L	60 in.
Mean Radius	$\bar{a}$	3.1725 in.
Wall Thickness	t	0.280 in.
Density		0.283 lbs/in^3
Young's Modulus	E	29.6*10^6 lbs/in^2
Poisson's Ratio		0.290
Inside Radius	a	3.0325 in.

Commercial Type: 6" ASA SCHEDULE 40/ STD BLACK/ASTM 53

II. Experimental Procedure

Figure VII shows a schematic representation of the instrumentation of the experimental model. For the data presented in this paper the following instrument checks were first accomplished with a vacuum tube voltmeter.

1. The output of the oscillator was adjusted to a set level, measurement taken at point (2).

2. The combined output of the oscillator and amplifier was then adjusted to a set level, measurement at point (3).

3. The voltmeter was then attached so as to measure the output of the accelerometer preamplifier (gain of unity) which was also an input to the oscilloscope, measurement at point (4).

The actual measurements of acceleration levels was then accomplished in the following manner. The accelerometer which used a magnet mount for attachment to the cylinder wall was placed on the surface of the cylinder. The frequency was then varied with the oscillator until a significant level of acceleration was observed. At this point the output of the amplifier was rechecked to insure that it had remained the same.

Acceleration readings were then taken in millivolts (rms) at one inch intervals in the axial direction and at intervals of 22½° in the circumferential direction,

Figure VII

Schematic of Experiment Instrumentation

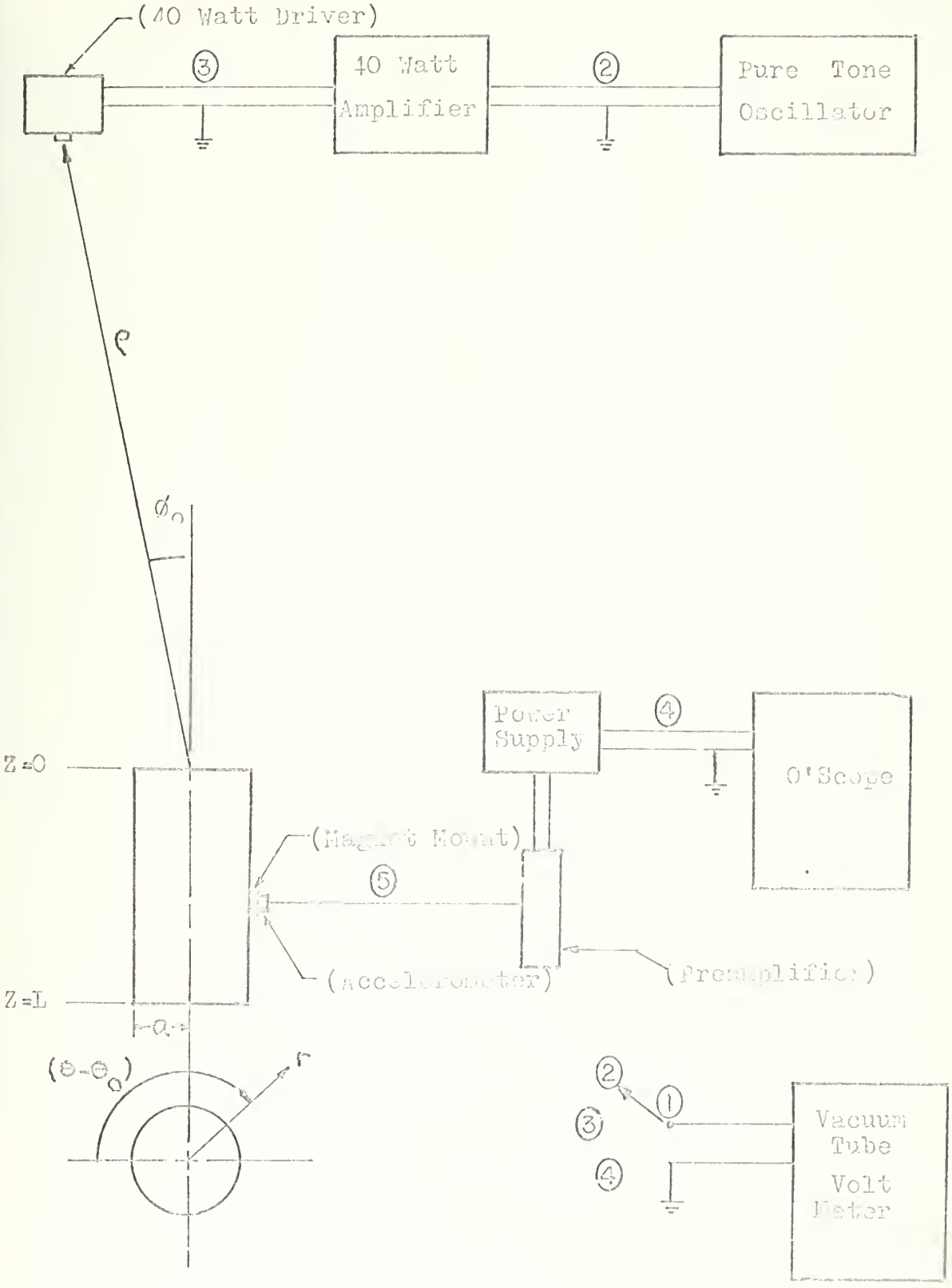

corresponding to sixteen equally spaced circumferential stations, see Figure VIII. This was accomplished by a grid network of tape laid out on the surface of the cylinder and marked at the proper intervals. The sensitivity of the accelerometer used was a constant 51 mv/g up to 4000 Hz. Above 4000 Hz. the magnet mounting device caused the sensitivity to become inaccurate and as a result the experiment was limited to a high frequency limit of 4000 Hz. Frequencies were determined by the oscilloscope display.

Figure VIII

Identification of
Circumferential Stations

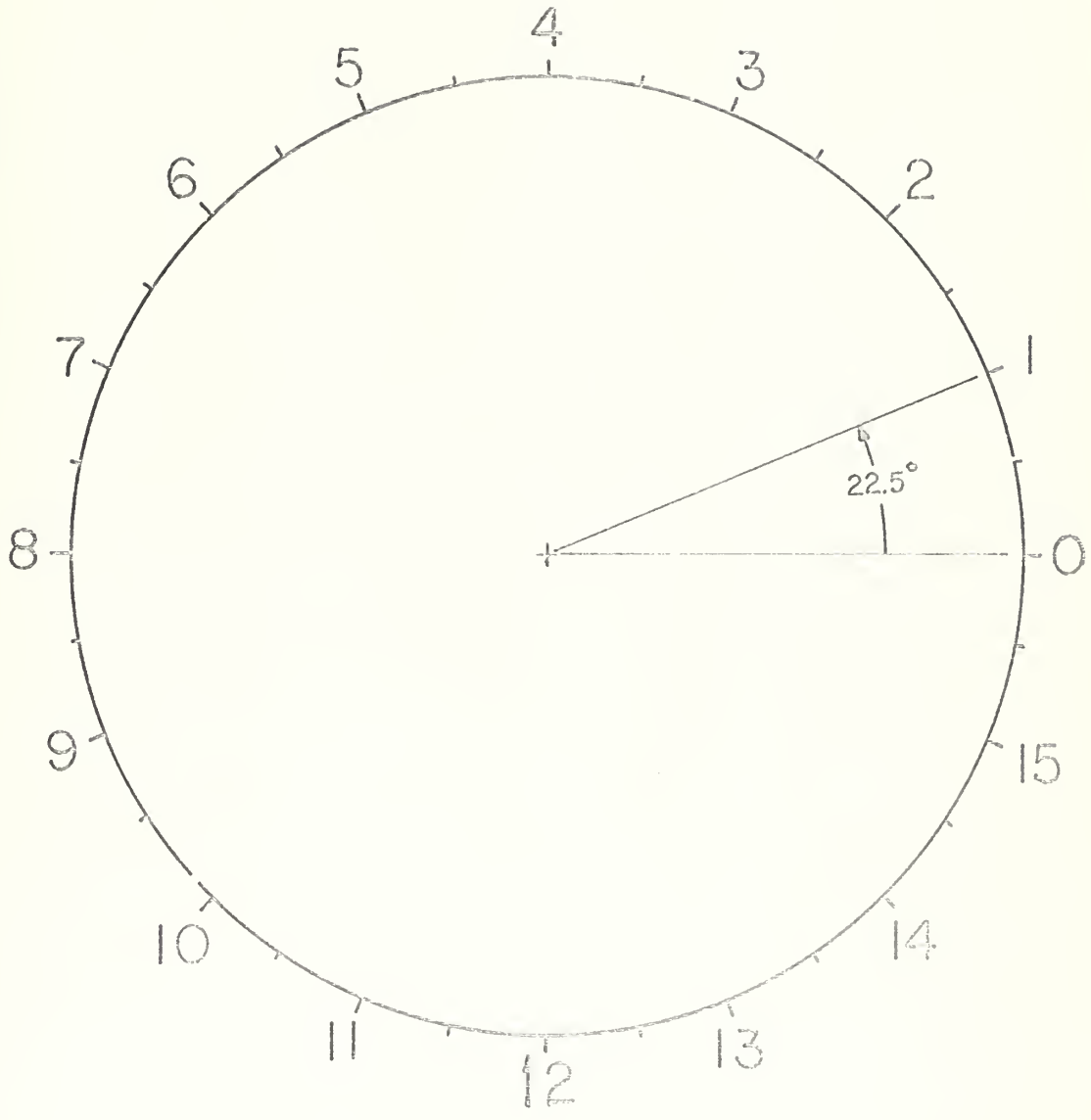

III. Analysis of Data

As previously stated rms acceleration levels were measured with an accelerometer along a tape grid which remained fixed throughout the series of experiments which resulted in the following data. Six different modes of significant acceleration levels were observed. These six modes are given in Table II in terms of the assumed experimental variables.

Tables III through VIII of Appendix A are the tabulation of the original rms acceleration levels recorded in millivolts (mv). The information presented at the top of each of those tables was arrived at after two steps of data reduction. These two steps are explained in detail in the following section.

A. Data Reduction Steps (1) and (2)

Step (1) Determination of Basic Vibration Pattern

It was assumed that the circumferential vibration pattern was of the form,

$$\cos n(\theta - \theta_o)$$

and similarily that the axial vibration pattern was of the form,

$$\cos \frac{m\pi z}{2L} - \sin \frac{m\pi z}{2L}$$

or equivalently,

$$\cos\left(\frac{\lambda z}{a} + \frac{\pi}{4}\right)$$

where λ is defined by Eq.(3).

Table II

Observed Modes

Frequency	Source Location	
f	ϕ_o	θ_o
Hz	( )°	Sta.#
1950	3°	8.5
2300	2°	3.5
2300	3°	8.5
3070	2°	3.5
3100	3°	8.5
3850	2°	3.5

At first glance it is obvious that there is a periodic pattern to the data in Tables III - VIII. It is an easy though tedious exercise to arrange this data in alternating positive and negative value groups. If this data so arranged is then transferred to a plot of amplitude versus position the basic cosine pattern is readily apparent. Define the following quantities,

$\bar{A}_{max}$: Maximum acceleration (rms) in the total vibration pattern.

$\bar{A}_{a,max}$: Maximum acceleration (rms) recorded at an axial station.

$\bar{A}_{a}$: Acceleration (rms) recorded at an axial station.

$\bar{A}_{c,max}$: Maximum acceleration (rms) recorded at a circumferential station.

$\bar{A}_{c}$: Acceleration (rms) recorded at a circumferential station.

Figures IX through XV then represent plots of normalized acceleration level versus position of measurement. Each plot represents the data for one of the six modes given in Table II. The position of nodes and antinodes can then be determined by simple examination of each individual plot. The actual determination of the nodes was performed on plots of too large a scale to be presented here. Table IX of Appendix A is a tabulation of the result of this determination.

Due to physical obstructions it was not possible to take axial measurements over the entire length of the cylinder. Thus m and as a result λ, were assumed to be given by the following relation,

$$m = \frac{2 \cdot L \quad (\text{in})}{\text{average node seperation (in)}}$$

The value of n was easily determined for each mode as it must of necessity be the number of nodes in the circumferential pattern.

Figure IX

Legend for Figures X through XV .

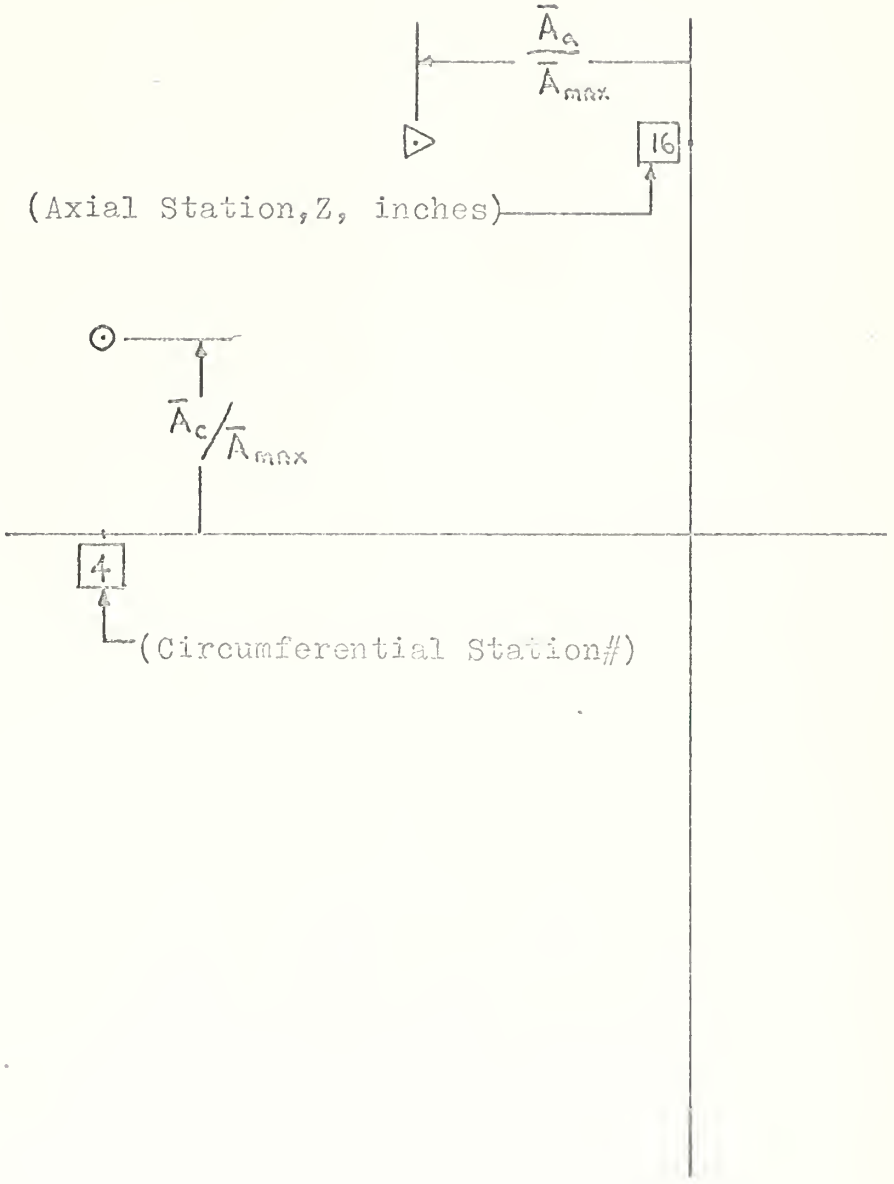

Figure X

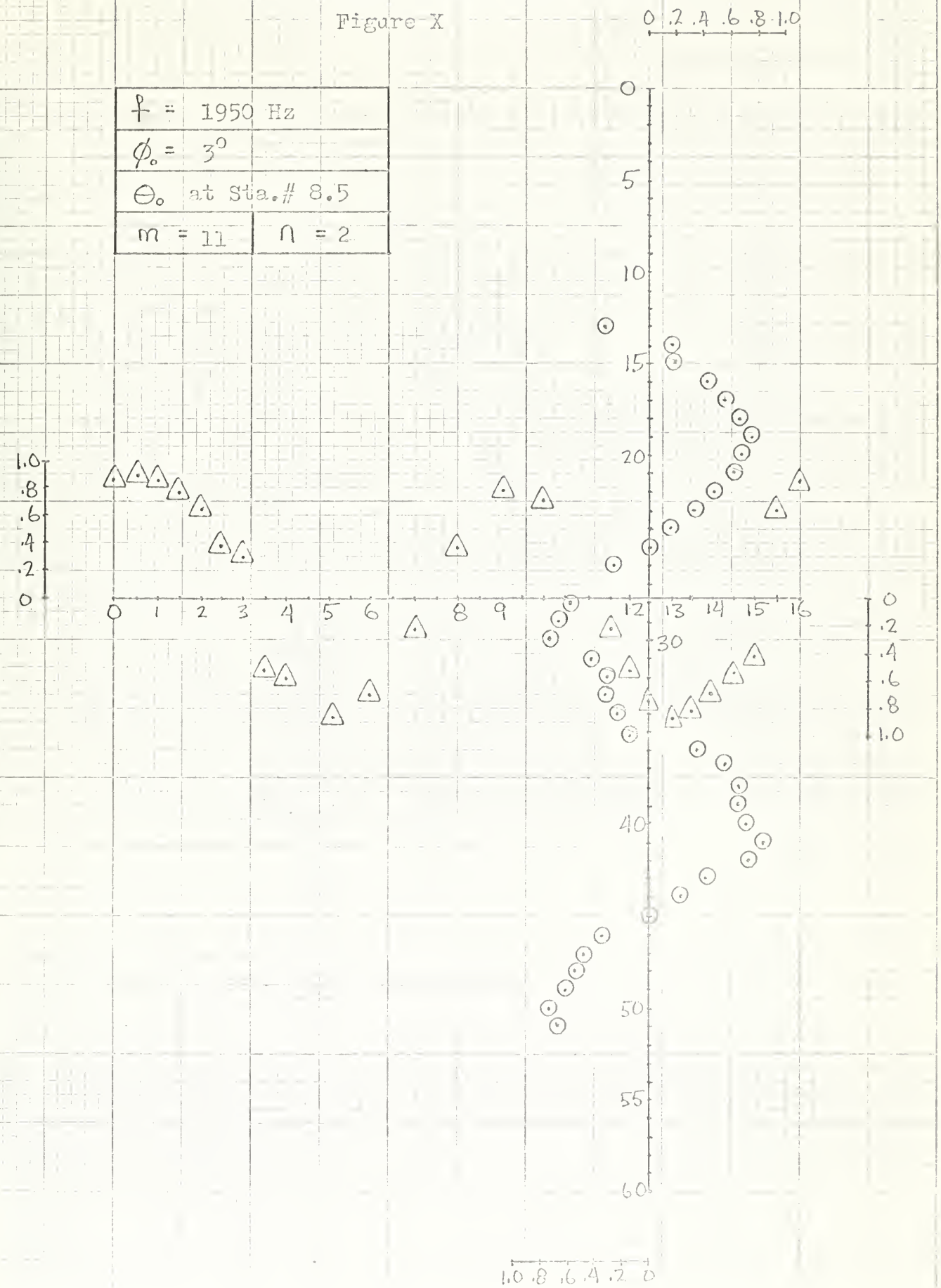
f = 1950 Hz
ϕ_o = 3°
Θ_o at Sta.# 8.5
m = 11
n = 2
0 .2 .4 .6 .8 1.0
0
5
10
15
20
30
40
50
55
60
1.0 .8 .6 .4 .2 0
0 1 2 3 4 5 6 8 9 12 13 14 15 16
1.0 .8 .6 .4 .2 0
0 .2 .4 .6 .8 1.0

Figure XI

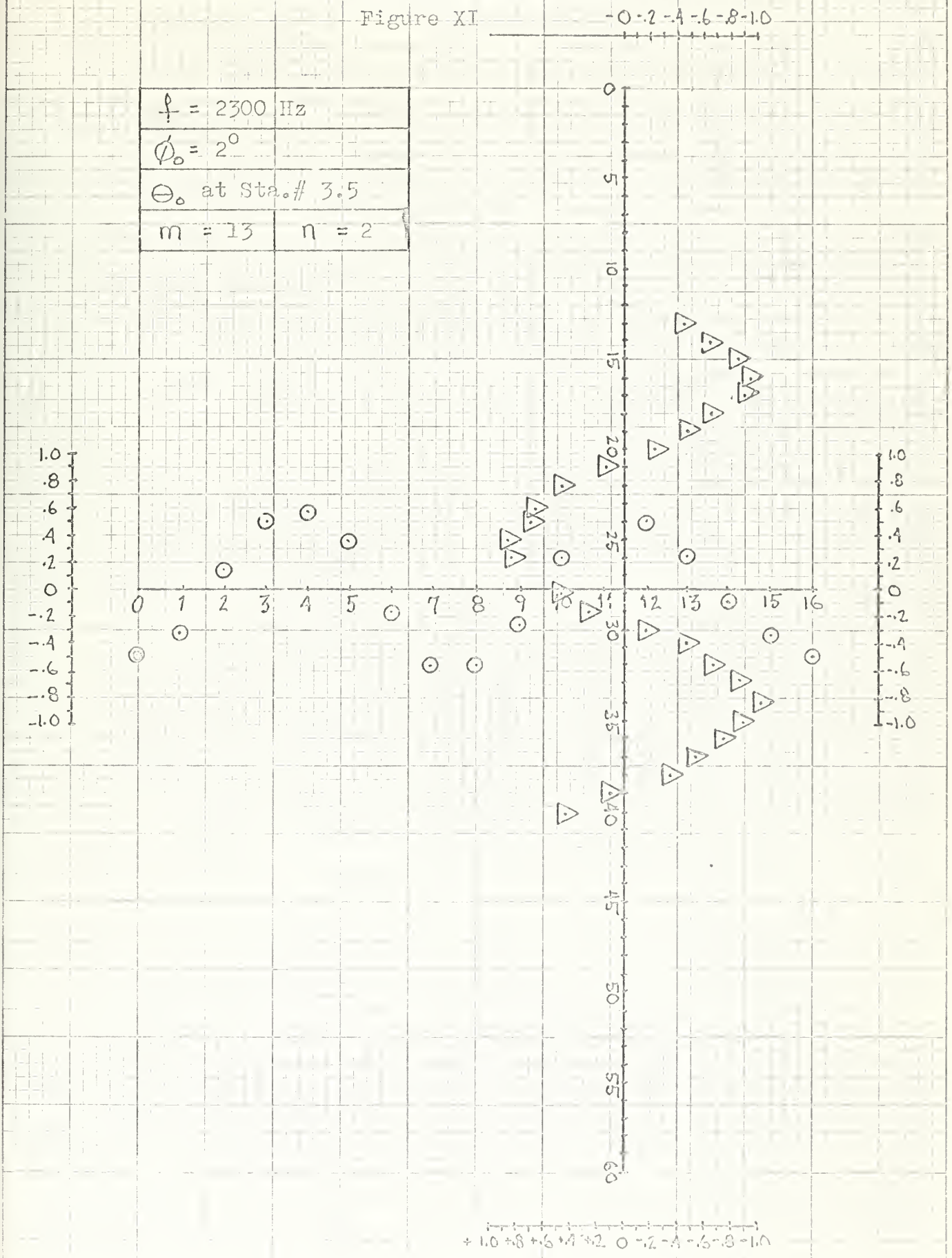

Figure XII

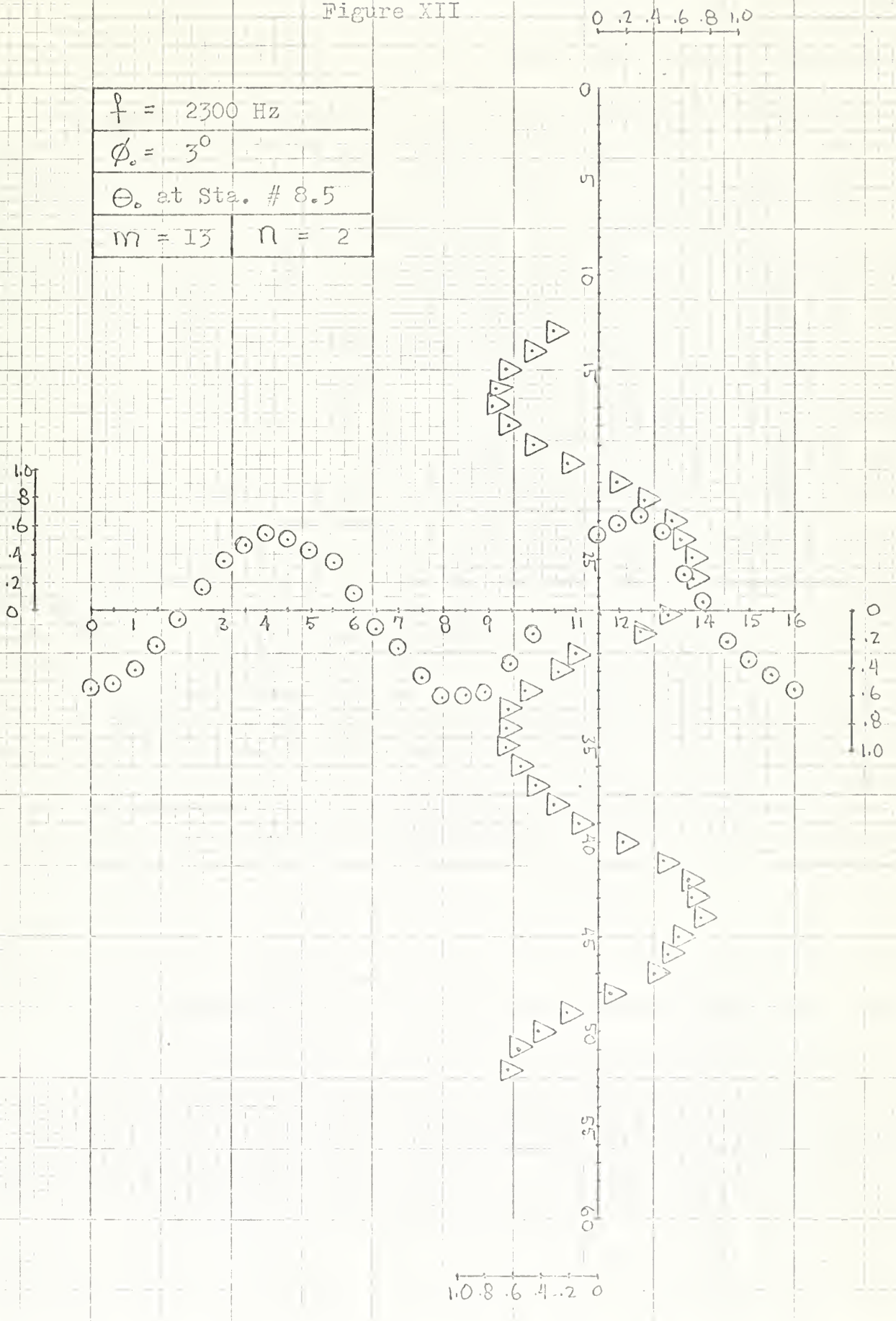
f = 2300 Hz
ϕ_o = 3°
Θ_o at Sta. # 8.5
m = 13
n = 2
0 .2 .4 .6 .8 1.0
0 5 10 15 20 25 30 35 40 45 50 55 60
1.0 .8 .6 .4 .2 0
0 1 2 3 4 5 6 7 8 9 11 12 14 15 16
1.0 .8 .6 .4 .2 0
0 .2 .4 .6 .8 1.0

Figure XIII

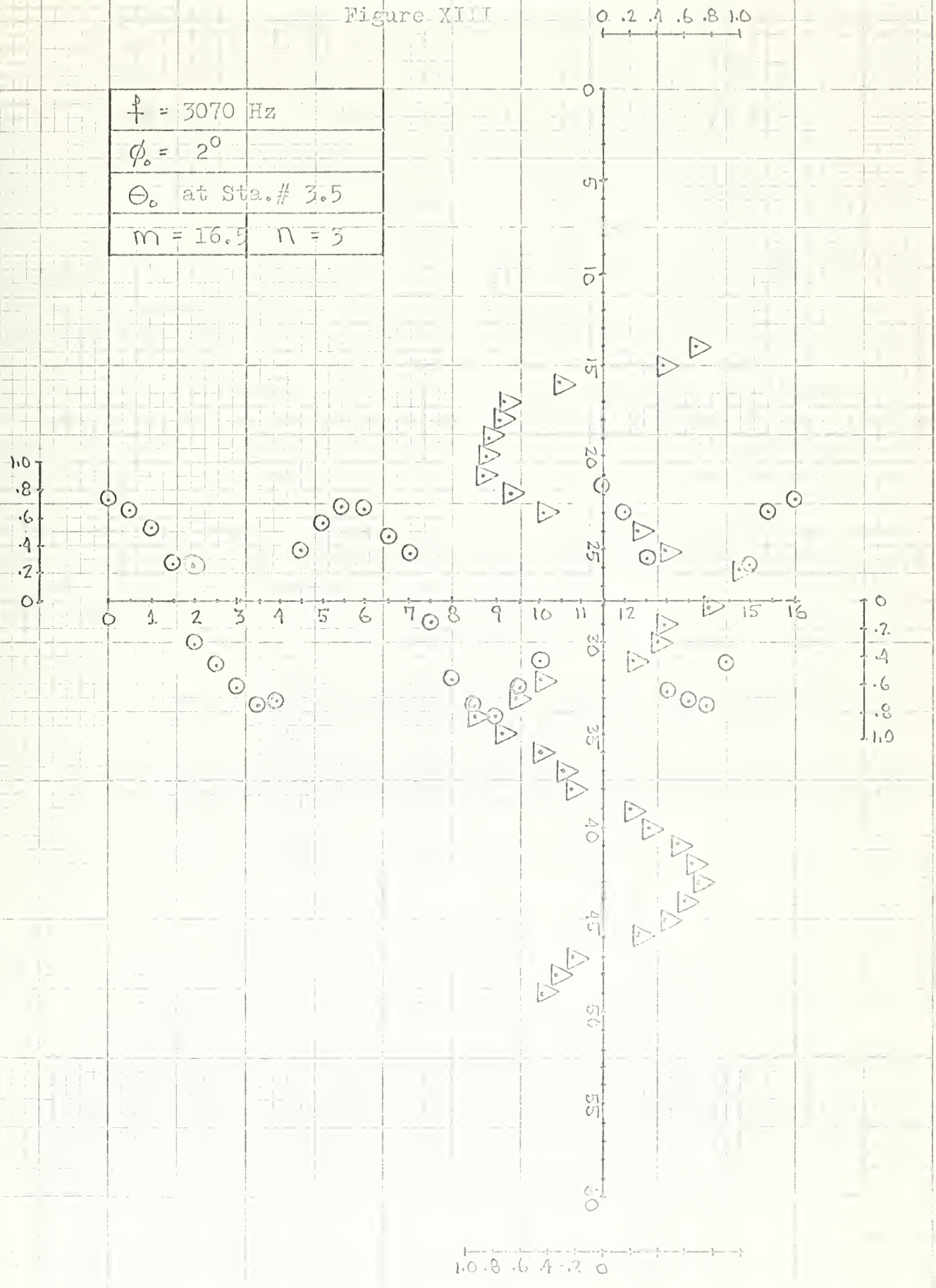
f = 3070 Hz
ϕ_o = 2°
Θ_o at Sta.# 3.5
m = 16.5 n = 3
0 .2 .4 .6 .8 1.0
1.0 .8 .6 .4 .2 0
0 1 2 3 4 5 6 7 8 9 10 11 12 15 16
0 5 10 15 20 25 30 35 40 45 50 55 60
0 .2 .4 .6 .8 1.0
1.0 .8 .6 .4 .2 0

Figure XIV

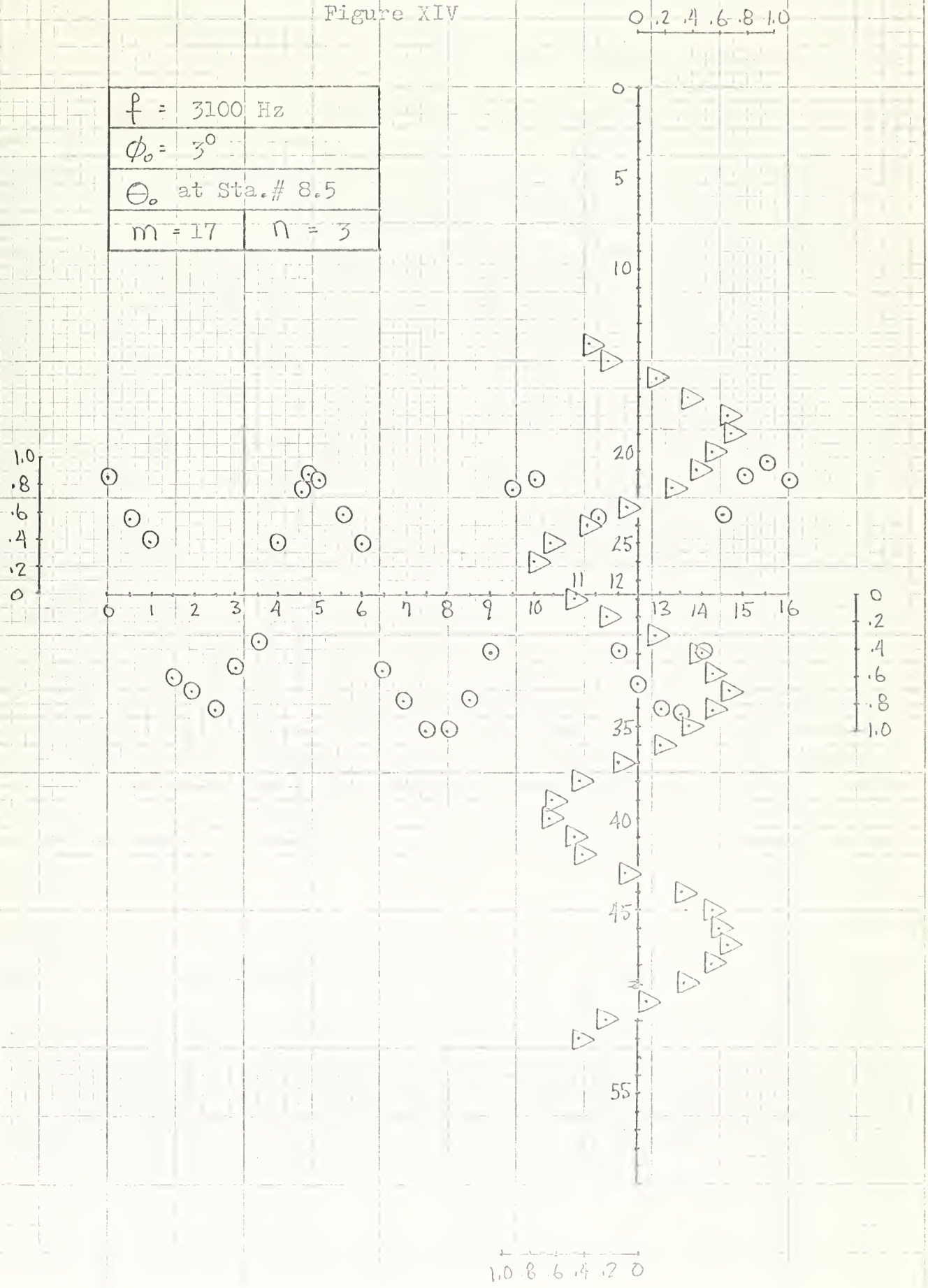
f = 3100 Hz
ϕ_o = 3°
Θ_o at Sta. # 8.5
m = 17
n = 3
0 .2 .4 .6 .8 1.0
0
5
10
20
25
11 12
35
40
45
55
1.0 .8 .6 .4 .2 0
0 1 2 3 4 5 6 7 8 9 10 13 14 15 16
1.0 .8 .6 .4 .2 0
0 .2 .4 .6 .8 1.0

Figure XV

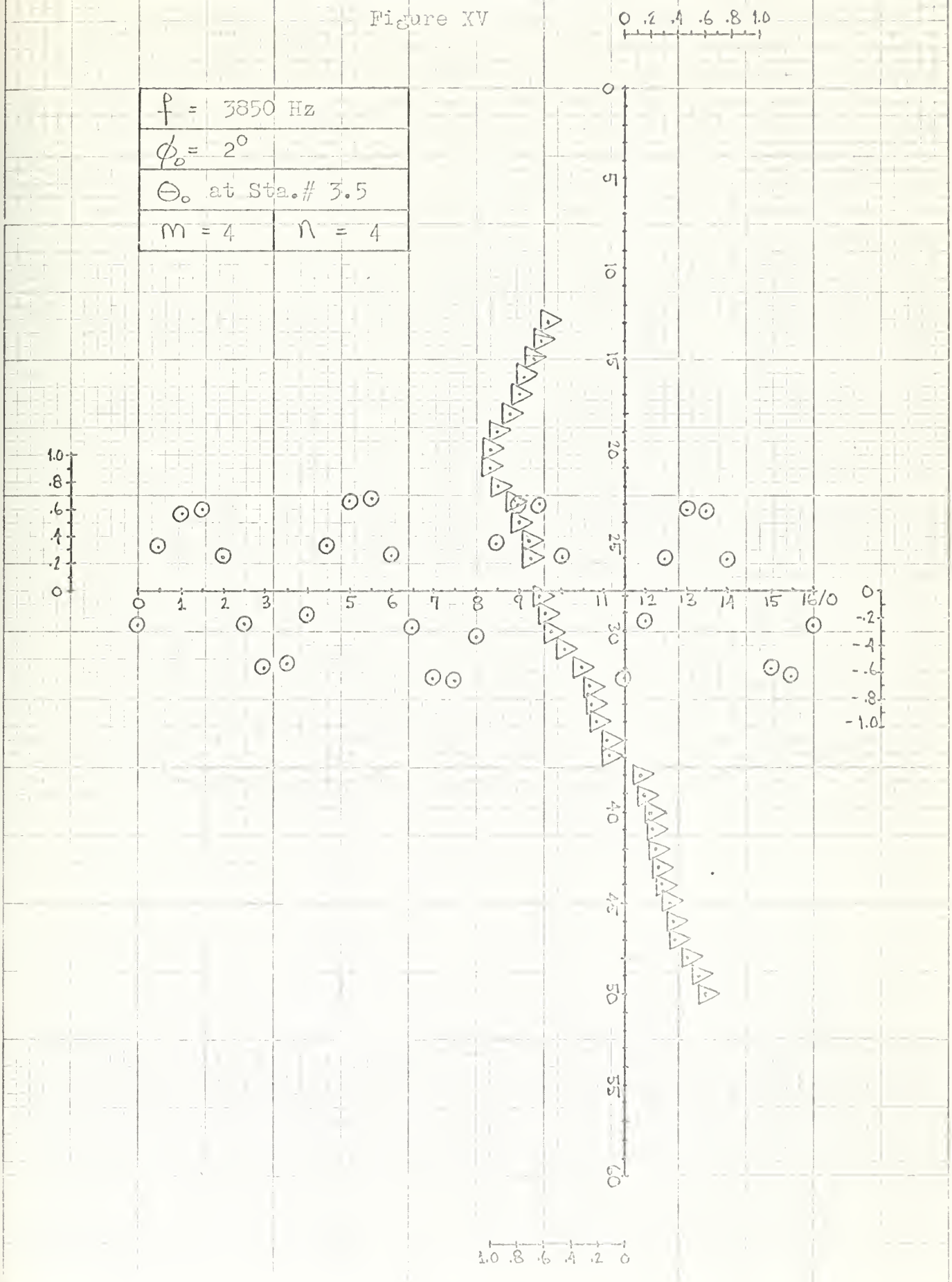
f = 3850 Hz
ϕ_o = 2°
Θ_o at Sta.# 3.5
m = 4
n = 4
0 .2 .4 .6 .8 1.0
1.0 .8 .6 .4 .2 0
0 5 10 15 20 25 30 35 40 45 50 55 60
0 1 2 3 5 6 7 8 9 11 12 13 14 15 16/0
0 -.2 -.4 -.6 -.8 -1.0

Step (2) Determination of $\bar{A}_{max}$, $\bar{V}_{max}$, $\bar{U}_{max}$.

The first calculation necessary for this step in the data reduction was to determine the maximum value of rms acceleration (mv) for each mode. If it is assumed that the vibration pattern is given by,

$$\bar{A}(z,\theta) = \bar{A}_{max} \cos n(\theta-\theta_o) \cos\left(\frac{m\pi z}{2L} + \frac{\pi}{4}\right)$$

then the axial measurements taken at $(\theta - \theta_o)_o$ must be of the form,

$$\bar{A}_a(z,(\theta-\theta_o)_o) = \bar{A}_{a,max} \cos n(\theta-\theta_o)_o \cos\left(\frac{m\pi z}{2L} + \frac{\pi}{4}\right)$$

and similarily the circumferential measurements taken at Z_o must be of the form,

$$\bar{A}_c(z_o,\theta) = \bar{A}_{c,max} \cos n(\theta-\theta_o) \cos\left(\frac{m\pi z_o}{2L} + \frac{\pi}{4}\right)$$

Now if Z_o is an antinode then we must have that

$$\bar{A}_{max} = \bar{A}_{c,max}$$

Similarily if $(\theta - \theta_o)_o$ is an antinode then,

$$\bar{A}_{max} = \bar{A}_{a,max}$$

Now if neither of these conditions has occurred then the simplest manner in which to proceed is as follows. Make an enlarged plot of the recorded data nearest the intersection of the axial and circumferential measuring lines, i.e., at the point defined by $(\theta - \theta_o)_o$, Z_o .

Define two angles, $0 \leq \alpha_c \leq \frac{\pi}{2}$

$$0 \leq \alpha_a \leq \frac{\pi}{2}$$

where $\begin{pmatrix} \alpha_c \\ \alpha_a \end{pmatrix}$ is the angular displacement in degrees of the nearest $\begin{pmatrix} \text{circumferential} \\ \text{axial} \end{pmatrix}$ node from the intersection point of the two measuring loci. In a similar fashion define two amplitudes $\begin{Bmatrix} (\bar{A}_c)_o \\ (\bar{A}_a)_o \end{Bmatrix}$ to be the acceleration level of the $\begin{Bmatrix} \text{Circumferential position} \\ \text{Axial Position} \end{Bmatrix}$ at the intersection point. Then $\bar{A}_{max}$ can be closely approximated by,

$$\bar{A}_{MAX} = \frac{(\bar{A}_c)_o + (\bar{A}_a)_o}{2 \sin \alpha_c \sin \alpha_a}$$

For three of the modes observed it was possible to take $\bar{A}_{max}$ directly from the data as an antinode occurred at the intersection point. The other three modes, though, required the use of the above technique to determine $\bar{A}_{max}$. The following three figures show this determination graphically.

Figure XVI

Legend for Figures XVII through XIX..

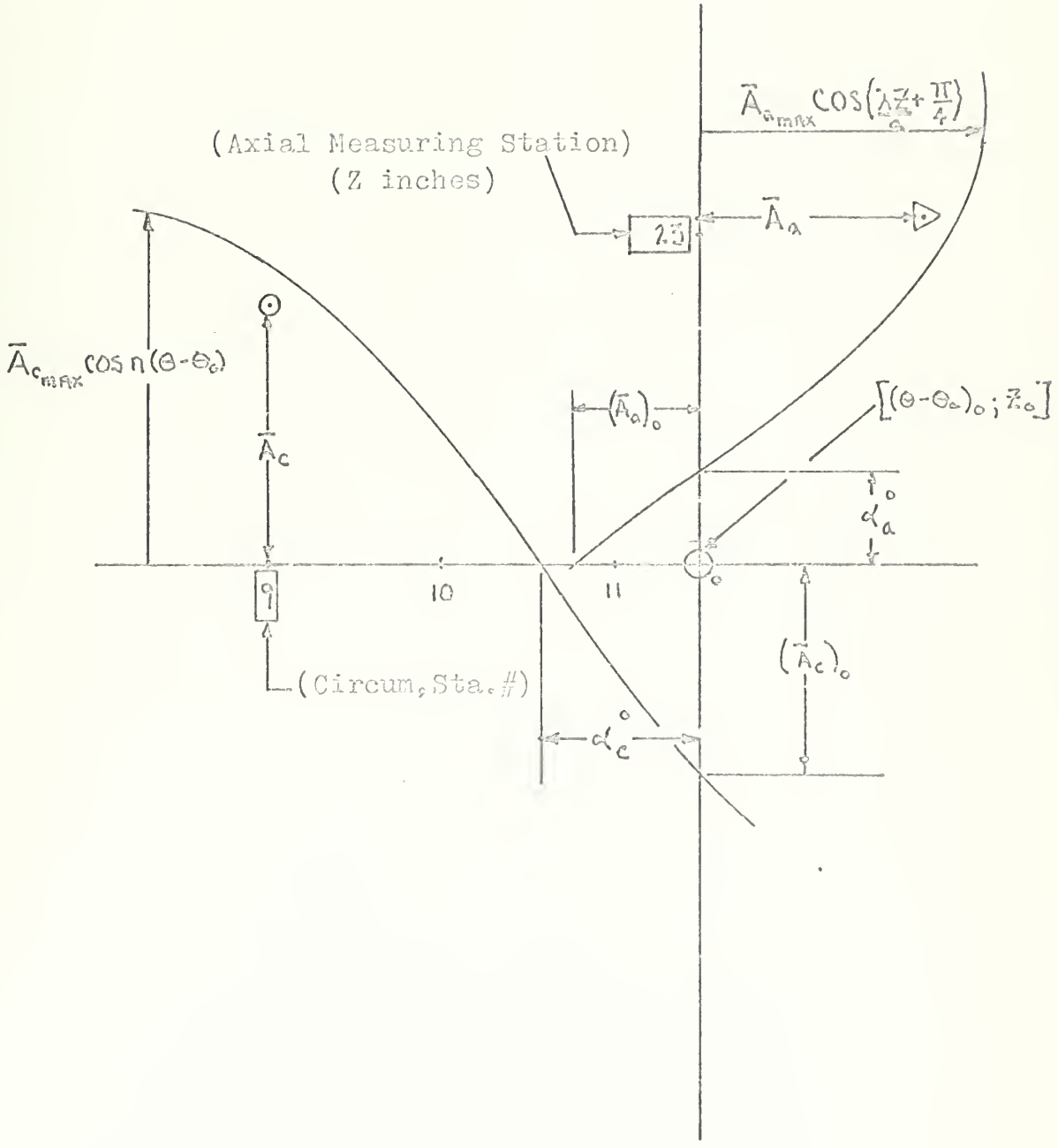

Figure XVII

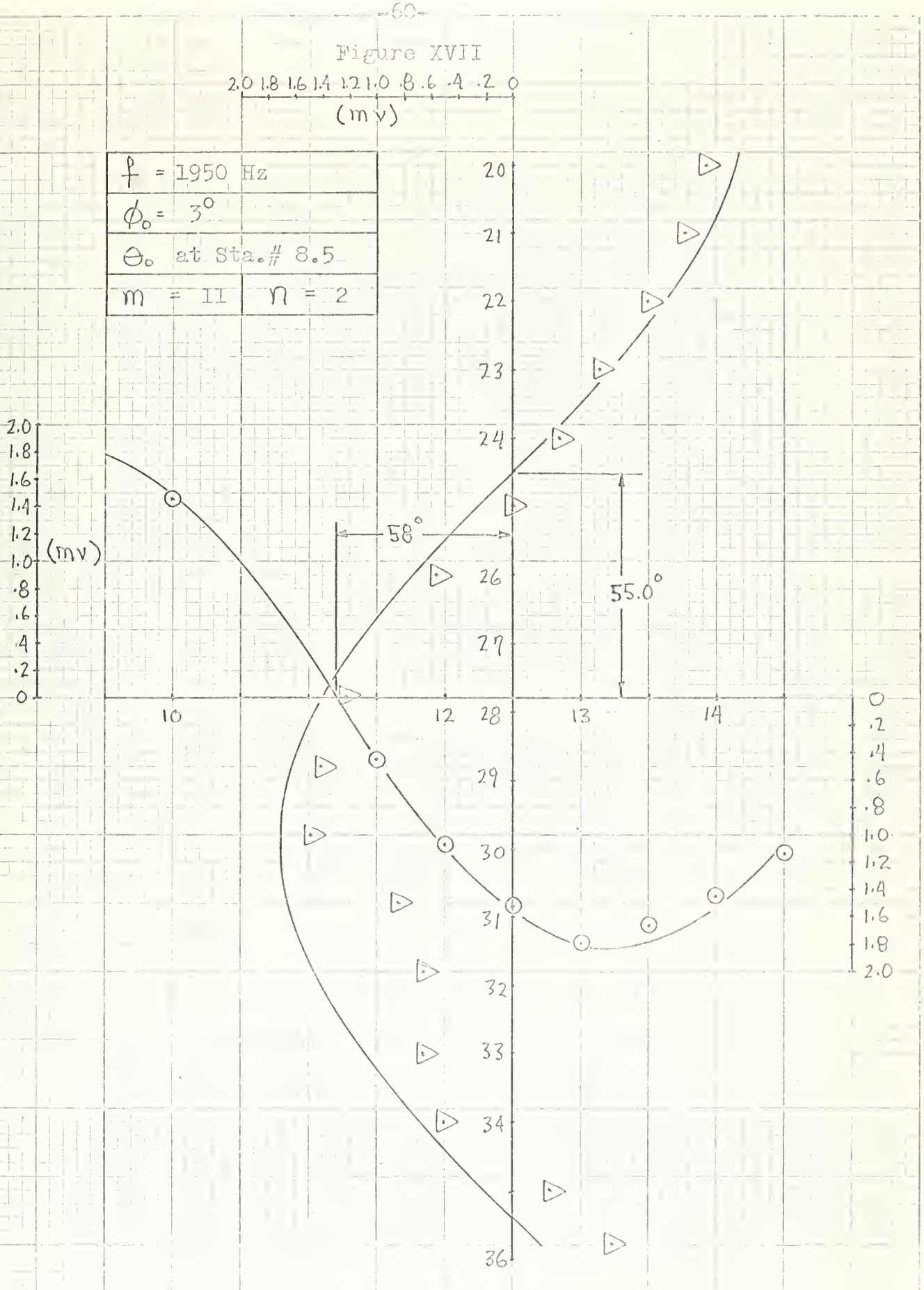
2.0 1.8 1.6 1.4 1.2 1.0 .8 .6 .4 .2 0
(mv)
f = 1950 Hz
ϕ_o = 3°
θ_o at Sta.# 8.5
m = 11
n = 2
20
21
22
23
24
26
27
28
29
30
31
32
33
34
36
58°
55.0°
2.0
1.8
1.6
1.4
1.2
1.0
.8
.6
.4
.2
0
(mv)
10
12
13
14
0
.2
.4
.6
.8
1.0
1.2
1.4
1.6
1.8
2.0

Figure XVIII

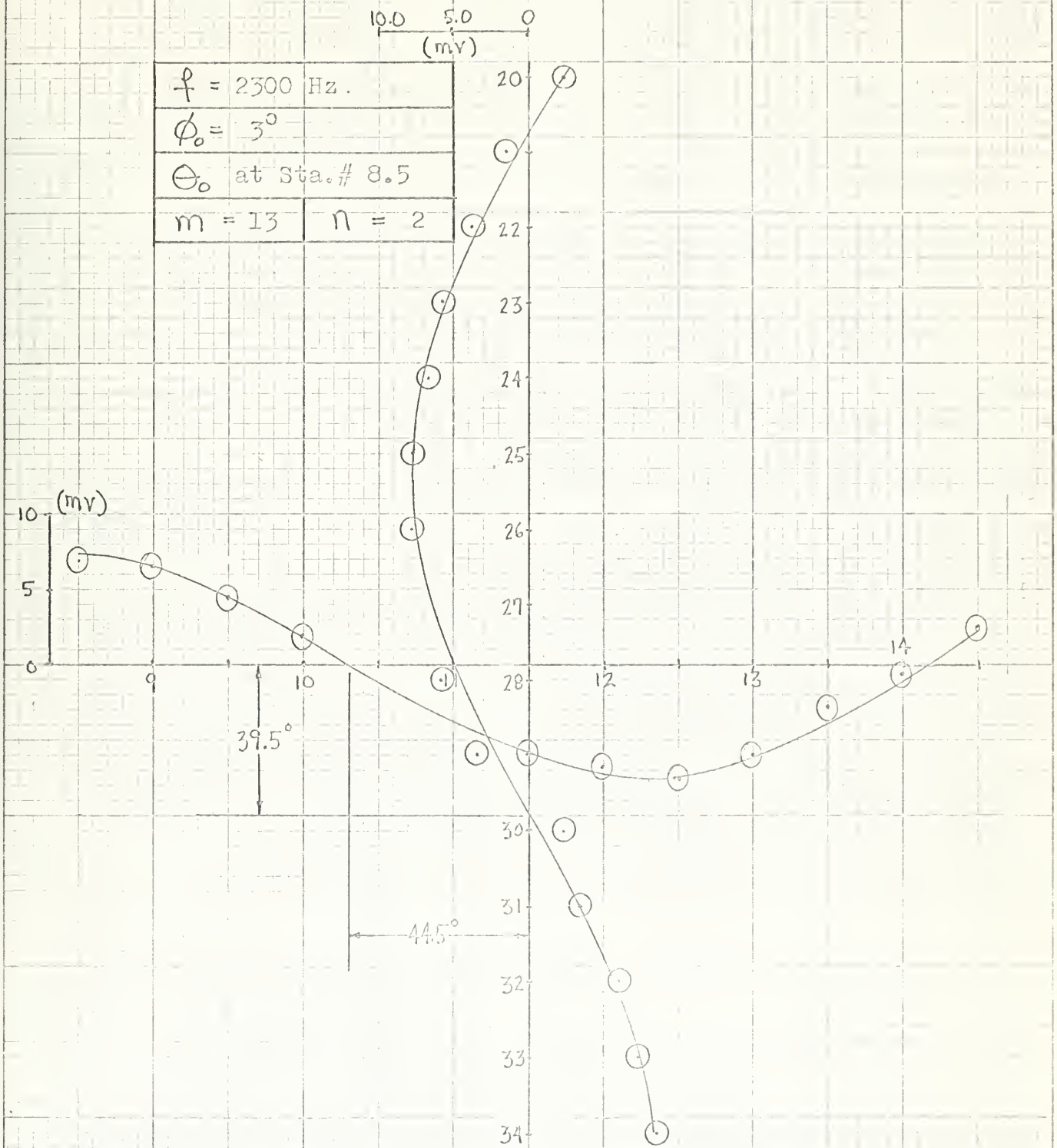

Figure XIX

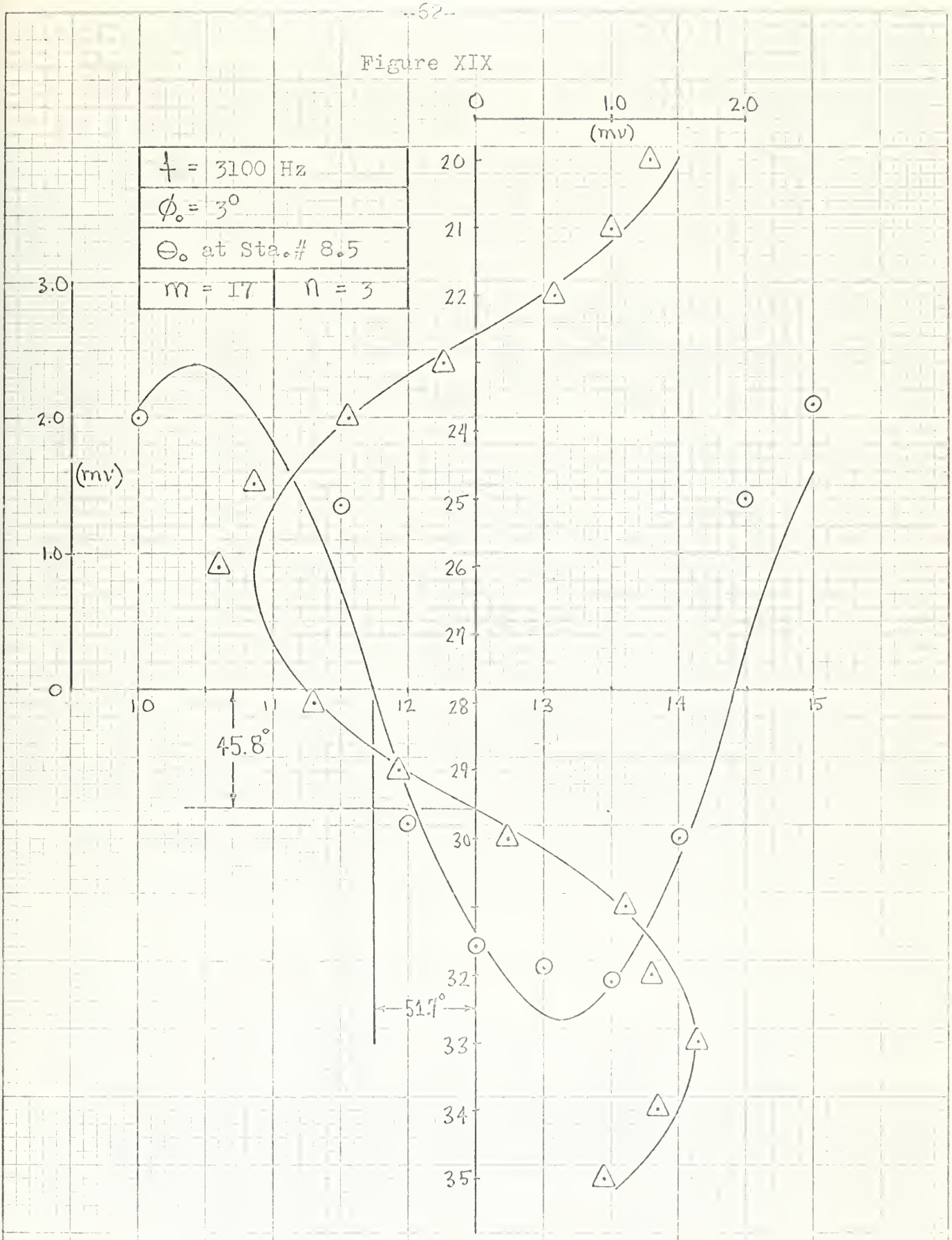
f = 3100 Hz
ϕ_o = 3°
Θ_o at Sta. # 8.5
m = 17
n = 3
0
1.0
2.0
(mv)
3.0
2.0
(mv)
1.0
0
20
21
22
24
25
26
27
28
29
30
32
33
34
35
10
11
12
13
14
15
45.8°
51.7°

ANALYSIS OF RESULTS

The first point upon which an analysis should be made is to what degree did the experimental analysis results prove or disprove the two fundamental purposes of the thesis, in light of the assumed variables frequency and source location. The two basic purposes of the thesis were to show that if significant vibration levels could be excited in a cylindrical duct by the presence of an internal sound field that these vibrations must be of the lobar type, and that if these vibration modes exist then there exists a coupling mechanism which will predict their occurrence.

I. Existence of Lobar Modes

The experimental analysis showed that for the frequency range examined that the only modes present with significant levels of vibration were in fact lobar modes with axially varying vibration patterns.

II. Validity of the Coupling Mechanism

The coupling mechanism as described in the theoretical conclusions may be examined on a number of points. The first and obvious comparison is accomplished by plotting the proper information from the reduced data portion of Tables III through VIII on Figure III of the theoretical conclusions. This has been done and the points are indicated by a $\triangle$. In each case the points are removed from the predicted value only by the variance in λ , except for the mode observed at 1950 Hz which

deserves special attention and will be discussed fully in the Conclusions.

The second comparison is the location of the nodes and antinodes of each mode, for the theory predicts their location also as a function of the source location. The theory predicts that the circumferential vibration pattern must be of the form,

$$\cos n(\theta - \theta_0)$$

and thus nodes must exist at,

$$\theta = \theta_0 + \frac{s\pi}{2n} \qquad s = 1, 3, \cdots, 2n-1$$

and antinodes at,

$$\theta = \theta_0 + \frac{s\pi}{2n} \qquad s = 0, 2, \cdots, 2n$$

Similarly the theory predicts that the axial vibration pattern must be of the form,

$$\cos\left(\frac{m\pi z}{2L} + \frac{\pi}{4}\right)$$

and thus nodes must exist at,

$$z\,(\text{in}) = \frac{30}{m}(2s-1) \qquad s = 1, 3, 5, \cdots$$

and antinodes at,

$$z\,(\text{in}) = \frac{30}{m}(2s-1) \qquad s = 0, 2, 4, \cdots$$

Thus it is seen that a shift in θ_0 must result in a shift in the circumferential nodal pattern. Figure 20 is a striking example of this phenomena and is a plot

of the normalized amplitude versus circumferential station spacing for the two modes observed at 2300 Hz. The points are data points and the curves are not fairings through these points but the actual cosine variation predicted by the theory. They are faired in each case only to their amplitude. The amplitudes of both patterns have been normalized by $\bar{A}_{max}$ ($\phi_o = 3^o$).

The other modes have been compared in a like manner and a result of this comparison is presented in Tables X through XV of Appendix A.

Figure 20

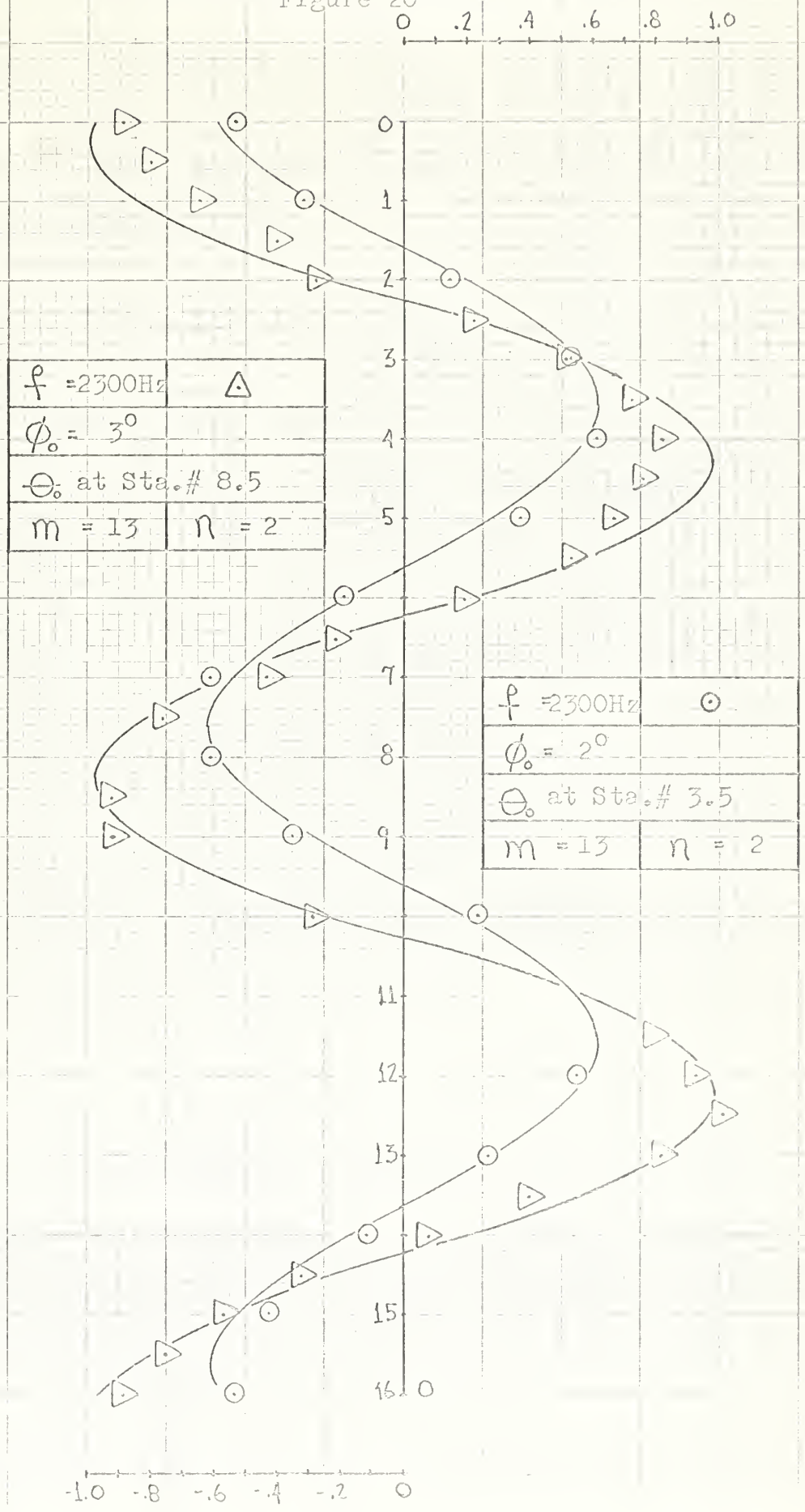
0 .2 .4 .6 .8 1.0
0
1
2
3
4
5
7
8
9
11
12
13
15
16
0
-1.0 -.8 -.6 -.4 -.2 0
f =2300Hz △
φ₀ = 3°
θ₀ at Sta.# 8.5
m = 13 n = 2
f =2300Hz ⊙
φ₀ = 2°
θ₀ at Sta.# 3.5
m = 13 n = 2

The second comparison that can be made in terms of the validity of the coupling parameter is what effect the variation of source location had on the amplitude of vibration. This can be attacked in the following way. In order to make any type of comparison utilizing the magnitude of the coupling parameter some assumptions must first be made concerning the modal impedance of the cylinder undergoing vibration. The subject of the variation in modal impedance with mode form, frequency and form of excitation is a lengthy subject and cannot be be gone into at great detail in this thesis if for no other reason than it was an item over which no control was maintained and no means were available for determining its effect upon the levels of vibration observed. This is primarily due to the real part of the radiation resistance a factor strongly coupled with the P_{rad} term of Eq.(48) which was completely neglected in the theory portion of the thesis. However it does not seem too presumptuous to assume that for the two pairs of modes that were observed at the same frequencies that the impedance remained constant, i.e., it is a constant with respect to amplitude of vibration. Thus a comparison can be made in the following manner. Assume that the modal impedance Z_{mn} is proportional to the ratio of the absolute value of the coupling parameter to the modal rms maximum velocity, (5), or;

$$|Z_{mn}| \sim |\chi_{mn}| \Big/ \overline{V}_{mn,max} \sim \text{CONSTANT}$$

Now if it assumed that for all the modes except the one observed at 1950 Hz, that the requirement,

$$K_{nq} = \frac{m\pi}{2L}$$

has been met then Eq.(54) becomes,

$$|\chi_{mn}| = \frac{L\pi a}{\sqrt{2}} J_n(\gamma_{nq} a)\, G_{nq}(Ka\phi_o)$$

where the values of G_{nq} are given by Eq.'s(30) through (32). Thus remembering that,

$$\beta = Ka\phi_o$$

that,

$$|\chi_{m2}| = C_1 (Ka)^3 \cdot (.0949)\, J_2(\gamma_{21} a)\, \phi_o^2$$

$$|\chi_{m3}| = C_1 (Ka)^4 \cdot (.0791)\, J_3(\gamma_{31} a)\, \phi_o^3$$

$$|\chi_{m4}| = C_1 (Ka)^5 \cdot (.6334)\, J_4(\gamma_{41} a)\, \phi_o^4$$

where,

$$C_1 = \frac{1.\pi C_o}{\sqrt{2}}$$

The value of these relations along with the other parameters needed to make the proper comparisons are given in Table XVI. The value for $|\chi_{mn}|$ for the mode observed at 1950 Hz was calculated in the following

Table XVI

f	n	ϕ_o^n	$J_n(\gamma_{mn}a)$	$(ka)^{n+1}$	$\frac{\lvert\chi_{mn}\rvert}{c_1}$	$\overline{V}_{mn,max}$
Hz	--	radians $*10^{-4}$	----	----	$*10^{-4}$	in/sec $*10^{-3}$
1950	2	27.5	.486	20.6	0.86	1.286
2300	2	12.1	.486	33.9	19.00	3.860
2300	2	27.5	.486	33.9	43.00	6.610
3070	3	42.2 $*10^{-2}$	.434	346.0	5.01	0.628
3100	3	144.0 $*10^{-2}$	.434	361.0	17.85	1.325
3850	4	147.0 $*10^{-4}$	.399	4590.0	17.00	3.130

manner. Eq.(11) was utilized to determine the mode wavenumber for this mode. It is then seen that the result of Eq.(11) is imaginary and therefore it is a damped mode. It can then be shown that the following approximation is accurate for, $e^{-(K_{pq}L)} \sim 0$,

$$\int_0^L \left(\cos\frac{m\pi z}{2L} - \sin\frac{m\pi z}{2L}\right) e^{-K_{pq}z}\, dz \sim \frac{L}{K_{pq}L + \frac{m\pi}{2}}$$

As stated before the most valid comparison based on these parameters will be the comparisons of modes at the same frequency and mode shape. Thus examining the two modes at 2300 Hz. first it can be seen that two comparisons might be made.

1) Using the experimental values of ϕ_o solve for the relationship,

$$\frac{V_{max}(\phi_o = 3^\circ)}{V_{max}(\phi_o = 2^\circ)} = \frac{|\chi_{mn}|(\phi_o = 3^\circ)}{|\chi_{mn}|(\phi_o = 2^\circ)}$$

and compare with the experimental value. The result of this comparison then is,

Predicted: 2.26 = (43.00/ 19.00)

Actual : 1.72 = (6.610/ 3.860)

2) Examine the relation, $|\chi_{mn}|/c_i V_{max}$ for constancy,

$\phi_o = 3^\circ$: .650 = ($43.00*10^{-4}/6.610*10^{-3}$)

$\phi_o = 2^\circ$: .492 = ($19.00*10^{-4}/3.86*10^{-3}$)

This same comparison may be also made for the two virtually identical modes observed at 3070 and 3100 Hz.

1) Solving for the velocity ratio;

Predicted : 3.56 (17.85/ 5.01)

Actual : 2.11 (1.325/ 0.628)

2) Checking $\frac{|X_{mn}|}{c_1}\Big/\bar{Y}_{mn,max}$ for constancy

$\phi_o = 3^o$: 1.345 = $(17.85*10^{-4}/1.325*10^{-3})$

$\phi_o = 2^o$: .798 = $(5.01*10^{-4}/0.628*10^{-3})$

Finally the other two modes not yet examined may be checked also for constancy of $\frac{|X_{mn}|}{c_1}\Big/\bar{Y}_{mn,max}$,

1950 Hz

$\phi_o = 3^o$: .067 = $(0.86*10^{-4}/1.286*10^{-3})$

3850 Hz

$\phi_o = 2^o$: .543 = $(17.00*10^{-4}/3.130*10^{-3})$

CONCLUSIONS

The analysis of results has shown that the two basic purposes of this thesis were accomplished. Lobar type structural vibration modes were excited in the cylindrical duct by a pure tone sound field and the theoretically derived coupling mechanism within limits predicted the frequency at which these modes would appear, the form they would take, the location of nodes and antinodes, and to a degree even predicted their relative amplitudes of vibration.

The prediction capability of the coupling mechanism however was weak in the area of predicting the axial vibration pattern that would be present at a resonant response frequency. The two obvious answers to this problem are at once evident.

(i) The experimentally observed structural modes were in actuality non-resonant modes.

(ii) The predicted theoretical modes were incorrect. For statement (i) to be true then it would seem that the resonant modes of the same lobar type should also have been observed experimentally. This did not occur. Therefore statement (ii) seems to be the answer to the problem. This is even easier to believe when it is realized that the assumptions made in adapting Arrold and Warburton's frequency equation to the experimental model were undoubtedly the greatest of any in the thesis. The actual shape

of the observed vibration patterns fit the theoretically assumed shape very nicely, but this does not imply that such an assumed shape should also give the same frequency result. A solution to the natural modes of vibration of a "Free-Free" cylinder with all end conditions properly satisfied would undoubtedly have a better fit to the data of this thesis than the solution used.

As was stated in the analysis of results little can be said about the capability of the coupling mechanism to predict relative strengths of vibration due to the unknown properties of the modal impedance. However the comparisons that were made in that section of the analysis were far better than would be expected considering the margin of slack that must exist to some degree in both the mechanism and the observed data and the powers that many of these quantities were raised to in order to make comparisons. Conclusions other than vibration level increases with increase in source offset angle should not be based on the present data. However it must be noted that this was not an initial desired result of the thesis.

Perhaps the most interesting result of the experimental analysis was the single non-predicted mode observed at 1950 Hz. This mode would seem to be a resonant cylinder mode if it is assumed that the modes at 2300 Hz were resonant modes. Also it is not necessarily correct to term it a non-predicted mode for the theory does predict a finite degree of coupling for modes not too far below

the cutoff frequency of interest. Another possibility for explanation presents itself if the mode observed at 3070 Hz is closely analyzed. For the purpose of analysis this mode was assumed to be identical with the 3100 Hz mode but in actuality its axial vibration pattern varied slightly from this sister mode and this is why in the data tables it is attributed with a value of m = 16.5, a not too plausible value but the one that best fits it nevertheless. Thus it is possible that this is in actuality the same type of mode as that observed at 1950 Hz. It must be noted that the 1950 Hz mode best fit the m = 11 vibration pattern which is the next level below the m = 13 pattern of the 2300 Hz modes. Thus the interesting phenomena that would seem to present itself, and does not seem too unreasonable, is that the cutoff frequency is not necessarily a constant value but rather might be of a fluctuating or finite bandwidth character, allowing close frequencies of vibration on either side of it to sway it from its path so to speak. This phenomena is definitely an item that deserves further study, both theoretically and experimentally.

RECOMMENDATIONS

The logical first recommendation would be to continue the experimental analysis over a wider range of frequencies and with cylinders of varying dimensions and mechanical properties. This should be done in conjunction with a better solution to the natural frequencies of cylinder vibration, the best approach probably being to adapt the experimental model to a specific theory.

A second recommendation which should offer interesting results would be to excite the cylinder with noise rather than pure tone sound.

A third recommendation already stated in the conclusions would be to investigate the cause and occurrence of modes of the type observed at 1950 Hz.

APPENDIX

Appendix A

Table III through Table VIII

Tabulation of original data in millivolts (mv) and summary of mode characteritics.

Table IX

Tabulation of observed nodes and antinodes.

Table X through Table XV

Comparison in tabular form of location of observed and predicted nodes and antinodes.

Table III

n = 2	m = 11	f = 1950 Hz
$\bar{A}_{max}$ = 15.75 in/sec^2	λ = 0.914	$\Delta^{\frac{1}{2}}$ = 0.319
$\bar{V}_{max}$ = 1.286*10^{-3} in/sec	ϕ_o = 3°	
$\bar{U}_{max}$ = 0.105*10^{-6} in	θ_o at Circumferential Sta.# 8.5	

Axial Waves

Z inches	Accel. mv	Z inches	Accel. mv
13	0.64	41	1.75
14	0.36	42	1.50
15	0.40	43	0.85
16	0.85	44	0.50
17	1.10	45	0.00
18	1.35	46	0.70
19	1.52	47	1.00
20	1.42	48	1.10
21	1.28	49	1.25
22	1.00	50	1.68
23	0.64	51	1.65
24	0.34		
25	0.00		
26	0.56		
27	---		
28	1.23		
29	1.40		
30	1.48		
31	0.35		
32	0.65		
33	0.65		
34	0.50		
35	0.29		
36	0.72		
37	1.15		
38	1.35		
39	1.35		
40	1.45		

Circumferential Waves

Sta. #	Accel. mv	Sta. #	Accel. mv
0.0	1.75	8.0	0.80
0.5	1.85	8.5	---
1.0	1.80	9.0	1.65
1.5	1.60	9.5	---
2.0	1.30	10.0	1.45
2.5	0.80	10.5	---
3.0	0.63	11.0	---
3.5	1.05	11.5	0.46
4.0	1.22	12.0	1.08
4.5	---	12.5	1.52
5.0	1.82	13.0	1.80
5.5	---	13.5	1.68
6.0	1.45	14.0	1.45
6.5	---	14.5	1.15
7.0	0.43	15.0	0.85
7.5	---	15.5	1.30

Table IV

n = 2	m = 13	f = 2300 Hz
$\bar{A}_{max} = 57.50$ in/sec^2	$\lambda = 1.08$	$\Delta^{\frac{1}{2}} = .237$
$\bar{V}_{max} = 3.86*10^{-3}$ in/sec	$\phi_o = 2^o$	
$\bar{U}_{max} = 0.26*10^{-6}$ in	θ_o at Circumferential Sta.# 3.5	

Axial Waves

Z inches	Accel. mv	Z inches	Accel. mv
13	3.5		
14	5.3		
15	6.6		
16	7.6		
17	7.2		
18	6.0		
19	3.9		
20	1.8		
21	1.1		
22	3.9		
23	5.4		
24	5.6		
25	6.9		
26	6.5		
27	---		
28	3.8		
29	2.2		
30	1.3		
31	3.7		
32	5.3		
33	6.8		
34	7.6		
35	7.1		
36	6.1		
37	4.2		
38	2.6		
39	0.8		
40	3.5		

Circumferential Waves

Sta. #	Accel. mv	Sta. #	Accel. mv
0	4.0	8.0	4.6
0.5		8.5	
1.0	2.4	9.0	2.3
1.5		9.5	
2.0	1.1	10.0	1.7
2.5		10.5	
3.0	3.9	11.0	---
3.5		11.5	
4.0	4.6	12.0	4.0
4.5		12.5	
5.0	2.8	13.0	2.0
5.5		13.5	
6.0	1.4	14.0	0.9
6.5		14.5	
7.0	4.6	15.0	3.2
7.5		15.5	

Table V

$n = 2$	$m = 13$	$f = 2300$ Hz
$\bar{A}_{max} = 98.20$ in/sec^2	$\lambda = 1.08$	$\Delta^{\frac{1}{2}} = 0.237$
$\bar{V}_{max} = 6.61*10^{-3}$ in/sec	$\phi_o = 3^c$	
$\bar{U}_{max} = 0.445*10^{-6}$ in	θ_o at Circumferential Sta.# 8.5	

Axial Waves

Z inches	Accel. mv	Z inches	Accel. mv
13	3.6	41	5.4
14	5.6	42	7.2
15	7.6	43	7.5
16	8.2	44	8.2
17	8.6	45	6.7
18	7.2	46	5.8
19	5.4	47	4.6
20	2.4	48	1.0
21	1.5	49	2.5
22	3.7	50	4.8
23	5.7	51	6.7
24	6.8	52	7.2
25	7.8		
26	7.8		
27	---		
28	5.8		
29	3.4		
30	2.2		
31	3.4		
32	6.0		
33	7.2		
34	7.5		
35	7.5		
36	6.6		
37	5.2		
38	3.5		
39	1.7		
40	1.2		

Circumferential Waves

Sta. #	Accel. mv	Sta. #	Accel. mv
0.0	6.6	8.0	7.1
0.5	6.0	8.5	6.9
1.0	4.8	9.0	6.7
1.5	3.0	9.5	4.5
2.0	0.8	10.0	2.0
2.5	1.6	10.5	---
3.0	3.8	11.0	---
3.5	5.4	11.5	5.8
4.0	6.0	12.0	6.9
4.5	5.7	12.5	7.4
5.0	4.9	13.0	6.0
5.5	4.0	13.5	2.9
6.0	1.4	14.0	0.6
6.5	1.5	14.5	2.5
7.0	3.2	15.0	4.1
7.5	5.6	15.5	5.4

Table VI

n = 3	m = 16.5	f = 3070 Hz
$\bar{A}_{max}$ = 12.11 in/sec^2	λ = 1.37	$\Delta^{\frac{1}{2}}$ = 0.316
$\bar{V}_{max}$ = 0.628*10^{-3} in/sec	ϕ_o = 2^o	
$\bar{U}_{max}$ = 0.033*10^{-6} in	θ_o at Circumferential Sta.# 3.5	

Axial Waves

Z inches	Accel. mv	Z inches	Accel. mv
13	----	41	0.85
14	1.10	42	1.00
15	0.70	43	1.10
16	0.50	44	0.95
17	1.15	45	0.70
18	1.20	46	0.40
19	1.30	47	0.33
20	1.35	48	0.52
21	1.40	49	0.67
22	1.10	50	----
23	0.70		
24	0.40		
25	0.74		
26	1.60		
27	----		
28	1.25		
29	0.72		
30	0.64		
31	0.33		
32	0.75		
33	1.00		
34	1.50		
35	1.20		
36	0.77		
37	0.48		
38	0.39		
39	0.32		
40	0.52		

Circumferential Waves

Sta. #	Accel. mv	Sta. #	Accel. mv
0.0	1.15	8.0	0.95
0.5	1.05	8.5	1.25
1.0	0.85	9.0	1.30
1.5	0.42	9.5	1.00
2.0	0.50	10.0	0.70
2.5	0.77	10.5	----
3.0	1.00	11.0	----
3.5	1.20	11.5	1.30
4.0	1.15	12.0	1.00
4.5	0.60	12.5	0.50
5.0	0.90	13.0	1.05
5.5	1.10	13.5	1.15
6.0	1.05	14.0	1.20
6.5	0.75	14.5	0.75
7.0	0.52	15.0	0.42
7.5	0.25	15.5	1.05

Table VII

$n = 3$	$m = 17$	$f = 3100$ Hz
$\bar{A}_{max} = 25.77$ in/sec^2	$\lambda = 1.41$	$\Delta^2 = 0.319$
$\bar{V}_{max} = 1.325*10^{-3}$ in/sec	$\phi_o = 3^o$	
$\bar{U}_{max} = .057*10^{-6}$ in	θ_o at Circumferential Sta.# 8.5	

Axial Waves

Z inches	Accel. mv	Z inches	Accel. mv
13	---	41	1.20
14	0.85	42	1.00
15	0.38	43	0.24
16	0.26	44	0.75
17	0.90	45	1.30
18	1.60	46	1.45
19	1.70	47	1.60
20	1.30	48	1.30
21	1.00	49	0.82
22	0.59	50	0.10
23	0.22	51	0.62
24	0.95	52	1.10
25	1.65		
26	1.90		
27	---		
28	1.20		
29	0.59		
30	0.24		
31	1.10		
32	1.30		
33	1.65		
34	1.35		
35	0.95		
36	0.44		
37	0.31		
38	1.05		
39	1.55		
40	1.60		

Circumferential Waves

Sta. #	Accel. mv	Sta. #	Accel. mv
0.0	2.05	8.0	2.45
0.5	1.35	8.5	1.90
1.0	0.95	9.0	1.00
1.5	1.50	9.5	1.80
2.0	1.75	10.0	2.00
2.5	2.05	10.5	---
3.0	1.30	11.0	---
3.5	0.90	11.5	1.35
4.0	0.90	12.0	1.00
4.5	1.80	12.5	1.90
5.0	2.00	13.0	2.05
5.5	1.42	13.5	2.15
6.0	0.90	14.0	1.10
6.5	1.45	14.5	1.40
7.0	1.90	15.0	2.10
7.5	2.45	15.5	2.35

Table VIII

n = 4	m = 4	f = 3850 Hz
$\bar{A}_{max}$ = 75.67 in/sec^2	λ = 0.332	$\Delta^{\frac{1}{2}}$ = 0.396
$\bar{V}_{max}$ = 3.13*10^{-3} in/sec	ϕ_o = 2^o	
$\bar{U}_{max}$ = 0.129*10^{-6} in	θ_o at Circumferential Sta.# 3.5	

Axial Waves

Z inches	Accel. mv	Z inches	Accel. mv
13	5.8	41	2.0
14	6.1	42	2.1
15	6.8	43	2.3
16	7.5	44	2.6
17	7.9	45	3.2
18	8.5	46	3.5
19	9.6	47	3.7
20	10.0	48	4.6
21	10.0	49	5.2
22	9.5	50	6.0
23	8.1		
24	8.0		
25	7.4		
26	7.2		
27	---		
28	6.5		
29	6.0		
30	5.6		
31	4.7		
32	3.3		
33	2.8		
34	2.6		
35	2.1		
36	1.4		
37	1.3		
38	1.1		
39	1.4		
40	1.9		

Circumferential Waves

Sta. #	Accel. mv	Sta. #	Accel. mv
0.	2.6	8.0	3.3
0.5	3.3	8.5	3.4
1.0	5.8	9.0	6.2
1.5	6.0	9.5	6.4
2.0	2.5	10.0	2.6
2.5	2.3	10.5	---
3.0	5.6	11.0	---
3.5	5.4	11.5	6.3
4.0	1.9	12.0	2.1
4.5	3.3	12.5	2.2
5.0	6.7	13.0	6.0
5.5	6.8	13.5	5.9
6.0	2.7	14.0	2.2
6.5	2.8	14.5	---
7.0	6.3	15.0	5.8
7.5	6.6	15.5	6.2

Table IX

f = 1950		n = 2	
m = 11		$\phi_o = 3^o$	
θ_o at Station # 8.5			
Nodes		Antinodes	
Circum.	Axial	Circum.	Axial
Sta.#	Z (in)	Sta.#	Z (in)
2.7	14.2	0.5	19.0
7.4	25.0	4.5	30.0
11.0	35.2	9.0	41.0
15.1	45.0	13.0	50.0

f = 2300		n = 2	
m = 13		$\phi_o = 2^o$	
θ_o at Station # 3.5			
Nodes		Antinodes	
Circum.	Axial	Circum.	Axial
Sta.#	Z (in)	Sta.#	Z (in)
1.6	20.6	3.6	16.0
5.6	29.8	7.6	25.5
9.6	38.9	---	34.0
13.6	---	16.0	---

f = 2300		n = 2	
m = 13		$\phi_o = 3^o$	
θ_o at Station # 8.5			
Nodes		Antinodes	
Circum.	Axial	Circum.	Axial
Sta.#	Z (in)	Sta.#	Z (in)
2.3	11.5	0.3	17.0
6.3	20.8	4.3	26.2
10.3	29.8	8.3	34.5
14.3	39.6	12.3	44.0
	48.4		

f = 3070		n = 3	
m = 16.5		$\phi_o = 2^o$	
θ_o at Station # 3.5			
Nodes		Antinodes	
Circum.	Axial	Circum.	Axial
Sta.#	Z (in)	Sta.#	Z (in)
2.1	15.8	0.0	20.5
4.8	23.6	3.4	---
7.3	31.5	5.9	34.1
10.3	38.6	8.9	43.0
12.8	46.4	11.5	---
15.1	---	14.1	---

f = 3850		n = 4	
m = 4		$\phi_o = 2^o$	
θ_o at Station # 3.5			
Nodes		Antinodes	
Circum.	Axial	Circum.	Axial
Sta.#	Z (in)	Sta.#	Z (in)
0.2	37.2	1.5	21.0
2.2	---	3.2	---
4.2		5.2	
6.2		7.5	
8.2		9.3	
10.2		11.5	
12.2		13.3	
14.2		15.5	

f = 3100		n = 3	
m = 17		$\phi_o = 3^o$	
θ_o at Station # 8.5			
Nodes		Antinodes	
Circum.	Axial	Circum.	Axial
Sta.#	Z (in)	Sta.#	Z (in)
1.25	15.8	15.6	19.0
3.9	22.6	2.5	26.0
6.5	29.7	5.0	33.0
9.2	36.5	7.9	40.0
11.8	43.2	---	47.0
14.5	50.1	13.4	---

Table X

f = 1950 Hz				n = 11			
Θ_o at Sta.# 8.5				n = 2			
Nodes				Anti-nodes			
Circum.		Axial		Circum.		Axial	
Sta.#		Z-inches		Sta.#		Z-inches	
Actual	Theory	Actual	Theory	Actual	Theory	Actual	Theory
2.7	2.5	---	2.73	0.5	0.5	---	8.17
7.4	6.5	14.2	13.61	4.5	4.5	19.0	19.10
11.0	10.5	25.0	24.50	9.0	8.5	30.0	30.00
15.1	14.5	35.2	37.50	13.0	12.5	41.0	40.90
		45.0	46.40			50.0	51.80
		---	57.30				

Table XI

f = 2300 Hz				m = 13			
Θ_o at Sta.# 3.5				n = 2			
Nodes				Antinodes			
Circum.		Axial		Circum.		Axial	
Sta.#		Z-inches		Sta.#		Z-inches	
Actual	Theory	Actual	Theory	Actual	Theory	Actual	Theory
1.6	1.5	---	2.31	3.6	3.5	---	6.92
5.6	5.5	---	11.54	7.6	7.5	16.0	16.15
9.6	9.5	20.6	20.75	---	11.5	25.5	25.38
13.6	13.5	29.8	30.00	16.0	15.5	34.0	34.62
		38.9	39.20			---	43.84
		---	48.50			---	53.07
		---	57.70				

Table XII

f = 2300 Hz				m = 13			
θ_o at Sta.# 8.5				n = 2			
Nodes				Antinodes			
Circum.		Axial		Circum.		Axial	
Sta.#		Z-inches		Sta.#		Z-inches	
Actual	Theory	Actual	Theory	Actual	Theory	Actual	Theory
2.3	2.5	---	2.31	0.3	0.5	---	6.92
6.3	6.5	11.5	11.54	4.3	4.5	17.0	16.15
10.3	10.5	20.8	20.75	8.3	8.5	26.2	25.38
14.3	14.5	29.8	30.00	12.3	12.5	34.5	34.62
		39.6	39.20			44.0	43.84
		48.4	48.50			---	53.07
		---	57.70				

Table XIII

f = 3070				m = 16.5			
θ_o at Sta.# 3.5				n = 3			
Nodes				Antinodes			
Circum.		Axial		Circum.		Axial	
Sta.#		Z-inches		Sta.#		Z-inches	
Actual	Theory	Actual	Theory	Actual	Theory	Actual	Theory
2.1	2.16	----	1.82	0.0	0.83	----	5.46
4.8	4.83	----	9.10	3.4	3.50	----	12.70
7.3	7.50	15.8	16.25	5.9	6.17	20.5	20.00
10.3	10.17	23.6	23.60	8.9	8.84	----	27.3
12.8	12.84	31.5	30.90	11.5	11.51	34.1	34.5
15.1	15.51	38.6	38.30	14.1	14.18	43.0	41.8
		46.4	45.4			----	49.00
		----	52.7			----	56.4
		----	60.00				

Table XIV

f = 3100 Hz				m = 17			
θ_o at Sta.# 8.5				n = 3			
Nodes				Antinodes			
Circum.		Axial		Circum.		Axial	
Sta.#		Z-inches		Sta. #		Z-inches	
Actual	Theory	Actual	Theory	Actual	Theory	Actual	Theory
1.25	1.84	---	1.76	15.6	0.51	---	5.30
3.90	4.51	---	8.80	2.5	3.18	---	12.35
6.50	7.18	15.8	15.85	5.0	5.85	19.0	19.40
9.20	9.83	22.6	22.90	7.9	8.50	26.0	26.50
11.80	12.50	29.7	30.00	---	11.19	33.0	33.50
14.50	15.17	36.5	37.10	13.4	13.86	40.0	40.60
		43.2	44.10			47.0	47.60
		50.1	51.00			---	54.70

Table XV

f = 3850 Hz				m = 4			
θ_o at Sta.# 3.5				n = 4			
Nodes				Antinodes			
Circum.		Axial		Circum.		Axial	
Sta.#		Z-inches		Sta.#		Z-inches	
Actual	Theory	Actual	Theory	Actual	Theory	Actual	Theory
0.2	0.5	----	7.50	1.5	1.5	21.0	22.50
2.2	2.5	37.2	37.50	3.2	3.5	----	52.50
4.2	4.5			5.2	5.5		
6.2	6.5			7.5	7.5		
8.2	8.5			9.3	9.5		
10.2	10.5			11.5	11.5		
12.2	12.5			13.3	13.5		
14.2	14.5			15.5	15.5		

Appendix B

Computerized Solution of Arnold and Warburton(4) Frequency Equation for a Thin-Walled Cylinder Freely Supported at the Ends.

```
AN IV G LEVEL 0, 400 0          MAIN              DATE = 68126          07

      REAL L,K,K0,K1,K2
      READ(5,1)A,L,H,D,RHO,E
    1 FORMAT(F6.4,4X,F5.2,5X,3(F5.3,5X),F10.1)
      WRITE(6,2)
    2 FORMAT(1H1//16X,35HNATURAL MODES OF CYLINDER VIBRATION/
     112X,15HA = RADIUS (IN),2X,15HL = LENGTH (IN),
     22X,18HH = THICKNESS (IN)/12X,19HD = POISSON'S RATIO,
     32X,25HRHO = DENSITY (LBS/CU IN)/12X,
     431HE = YOUNG'S MODULUS (LBS/SQ IN)/12X,21HFREQ = FREQUENCY (K
     512X,32HN = NO. OF CIRCUMFERENTIAL WAVES/
     612X,27HM = NO. OF AXIAL HALF-WAVES//27X,10HINPUT DATA/)
      WRITE(6,3)A,L,H,D,RHO,E
    3 FORMAT(12X,4HA = ,F6.4,5X,4HL = ,F5.2,5X,4HN = ,F5.3/
     112X,4HD = ,F5.3,5X,6HRHO = ,F5.3,5X,4HE = ,E10.1/)
      WRITE(6,4)
    4 FORMAT(27X,11HOUTPUT DATA/13X,1HN,7X,1HM,8X,1HK,7X,5HSRDEL,
     16X,4HFREQ/)
      PI=3.1415928
      TOL=0.000001
      DO 25 N=2,4
      DO 25 L1=1,10
      M=L1-1
      RM=M
      RN=N
      K=A*PI*RM/L
    9 B1=(H**2)/(12.*A**2)
      B=B1
      Y11=K**2+(1.-D)*RN**2/2.
      Y12=-(1.+D)*K*RN/2.
      Y13=D*K
      Y23=-(RN+B*(RN**3+(2.-D)*K**2*RN))
      Y22=(1.+D)*K**2/2.+RN**2+B*(RN**2+2.*(1.-D)*K**2)
      Y33=1.+B*(K**2+RN**2)**2
      K0=-Y11*Y22*Y33-2.*Y12*Y23*Y13+Y13**2*Y22+Y12**2*Y33+Y23**2*Y
      K1=Y11*Y33+Y11*Y22+Y22*Y33-Y13**2-Y12**2-Y23**2
      K2=-Y11-Y22-Y33
      X0=-0.25
      DO 15 I=1,100
      F1=X0**3-K2*X0**2+K1*X0-K0
      F2=3.*X0**2-2.*K2*X0+K1
      X1=X0-F1/F2
      IF(ABS(X1-X0)-TOL)15,16,10
   10 X0=X1
   15 CONTINUE
   16 FREQ=SQRT(ABS(X0)*E*386.09/(12*RHO*(A+H)**2*(1.-D**2)))/(2000.*P
      X2=ABS(X0)
      X3=SQRT(X2)
   20 WRITE(6,21)RN,RM,K,X3,FREQ
```

```
   21    FORMAT(12X,2(F4.1,4X),2(F6.4,4X),F7.4)
   25    CONTINUE
         END
```

NATURAL MODES OF CYLINDER VIBRATION

A = RADIUS (IN) L = LENGTH (IN) H = THICKNESS (IN)
D = POISSON'S RATIO RHO = DENSITY (LBS/CU IN)
E = YOUNG'S MODULUS (LBS/SQ IN)
FREQ = FREQUENCY (KC)
N = NO. OF CIRCUMFERENTIAL WAVES
M = NO. OF AXIAL HALF-WAVES

INPUT DATA

A = 3.1725 L = 60.00 H = 0.280
D = 0.290 RHO = 0.283 E = 29600000.0

OUTPUT DATA

N	$\frac{M}{2}$	K λ	SRDEL $\Delta^{1/2}$	FREQ
2.0	0.0	0.0	0.0683	0.6610
2.0	1.0	0.1661	0.0798	0.7720
2.0	2.0	0.3322	0.1089	1.0539
2.0	3.0	0.4983	0.1489	1.4407
2.0	4.0	0.6644	0.1960	1.8971
2.0	5.0	0.8306	0.2480	2.4000
2.0	6.0	0.9967	0.3027	2.9294
2.0	7.0	1.1628	0.3583	3.4677
2.0	8.0	1.3289	0.4133	4.0000
2.0	9.0	1.4950	0.4665	4.5148
3.0	0.0	0.0	0.1932	1.8693
3.0	1.0	0.1661	0.1958	1.8950
3.0	2.0	0.3322	0.2038	1.9725
3.0	3.0	0.4983	0.2173	2.1025
3.0	4.0	0.6644	0.2361	2.2846
3.0	5.0	0.8306	0.2600	2.5157
3.0	6.0	0.9967	0.2883	2.7905
3.0	7.0	1.1628	0.3205	3.1016
3.0	8.0	1.3289	0.3556	3.4412
3.0	9.0	1.4950	0.3928	3.8011
4.0	0.0	0.0	0.3703	3.5839
4.0	1.0	0.1661	0.3716	3.5961
4.0	2.0	0.3322	0.3754	3.6331
4.0	3.0	0.4983	0.3819	3.6957
4.0	4.0	0.6644	0.3911	3.7847
4.0	5.0	0.8306	0.4021	3.8912
4.0	6.0	0.9967	0.4150	4.0155
4.0	7.0	1.1628	0.4358	4.2176
4.0	8.0	1.3289	0.4564	4.4165
4.0	9.0	1.4950	0.4795	4.6407

BIBLIOGRAPHY

1. Morse, P.M., Vibration and Sound , (McGraw-Hill Book Company, Inc., New York, 1948), p.305.

2. Noble, B., Methods Based on the Weiner-Hopf Technique, (Pergamon Press, New York, 1958), p.116.

3. Greenspon, J.E., J. Acoust. Soc. Am., 32,1960, p.571.

4. Arnold, R.N.; Warburton, G.B., Proc. Royal Soc. (london) A197, 1949, p. 238.

5. Smith, P.W. Jr.; Lyon, R.H., Sound and Structural Vibration, (Bolt Beranek and Newman Inc., 1964),p. 151-166.

6. Timoshenko, S., Vibration Problems in Engineering , (D. Van Nostrand Company, Inc., New York, 1955), p.336

7. Timoshenko, S., Theory of Plates and Shells, (McGraw-Hill Book Company, Inc., New York, 1940), p.389.

8. Rayleigh, J.W.S., The Theory of Sound, (Dover Publications, Inc., New York, 1945), 1 , p.399.